HIGH DETECTIVITY PYROELECTRIC INFRARED SENSOR

by

ANNAND BALASUBRAMANIYAM

Presented to the Faculty of the Graduate School of

The University of Texas at Arlington in Partial Fulfillment

of the Requirements

for the Degree of

MASTER OF SCIENCE IN ELECTRICAL ENGINEERING

UNIVERSITY OF TEXAS ARLINGTON

DECEMBER 2010

ACKNOWLEDGEMENTS

I would like to express my gratitude and appreciation to my advising professor Dr. Donald Butler, not only for his continuous support and guidance but also for his encouragement and motivation throughout the course of this work. During my work from May 2009, he gave me the freedom to talk and discuss with him anytime about any aspect of the research. He gave me full freedom to work in every possible aspect of the project and come up with new ideas. The confidence he had in me helped my complete this project on time and achieve this goal.

I would also like to thank Dr. Michael Vasilyev and Dr.W.Alan Davis for being on this committee and the time they have spent for reviewing the thesis and providing my helpful suggestions.

I would like to thank my friends and co-workers Suraj Patel, Rohit and Gaviraj for their help and support. I would like to thank my colleagues in the Microsensors and noise lab for their support and companionship.

I would like to show my gratitude and thank my father Rajan Balasubramaniyam, my mother VijayaLakshmi Balasubramaniyam, my sister Anuradha Nirmal and Brother in-law Nirmal Govindan for their financial and mental support during difficult times of the coursework. They have guided me and instilled the confidence in me to make this dream come true.

December 16, 2010

ABSTRACT

HIGH DETECTIVITY PYROELECTRIC INFRARED SENSOR

Annand Balasubramaniyam

The University of Texas Arlington 2010

Supervising Professor: Donald P. Butler

The sensors which measure physical quantities by sensing them as thermal quantities and then converting the thermal signals into electrical signals are called thermal sensors. One such type of thermal sensor is a pyroelectric infrared sensor. Thermal sensors are not popular mainly because they are slow devices, and they have low sensitivity when compared to photon detectors. One major advantage of thermal detectors over photon detectors is that they can operate at room temperature. This is one of the main motivations for this research. The aim of the thesis is to design an uncooled, high detectivity pyroelectric infrared detector. The high detectivity is obtained by reducing the thermal conductivity from the sensor to the substrate or the heat sink. Pyroelectricity is defined as the change in polarization with corresponding change in temperature. Lead calcium titanate (PCT) is a material which is a ferroelectric perovskite. It has a very high pyroelectric co-efficient, high dielectric constant and if deposited in a proper ratio could yield a very high pyroelectric response in the range of 6 $x10^{6}$ V/W. The thermal conductance between the sensor and the substrate using the proposed design is found to be as low as $9.51x10^{-9}$ W/K, less than the radiative thermal conductance $3.69x10^{-7}$ W/K. Two kinds of absorber designs are proposed with this detector. The efficiency of the design and the directivity

of the top surface of the infrared sensor are found to have 55° field of view on both sides. Various fabrication methods for fabricating the device have been discussed in detail and the best methods have been mentioned in comparison over the other types. The development of the absorber and its application in the detection mechanism is discussed in detail.

TABLE OF CONTENTS

ACKNOWLEDGEMENTS iii

ABSTRACT iv

LIST OF ILLUSTRATIONS viii

LIST OF TABLES x

Chapter Page

1 INTRODUCTION 1

1.1 Overview 1

1.2 Infrared Radiation 1

1.3 Applications of IR detectors 3

1.4 Selection of IR detectors 5

1.5 Types of IR detectors 5

1.6 Photon detectors 6

1.7 Thermal Detectors 7

1.8 Motivation and Goals 12

1.9 Organization of the Document 13

2 PYROELECTRICITY 14

2.1 Overview 14

2.2 Voltage Responsivity 19

2.3 Noise Mechanisms 20

2.4 Noise Equivalent Power 21

2.5 Other effects 22

2.6 Modes of Operation 23

2.7 Conclusions 23

3 PYROELECTRIC SENSOR DESIGN 25

3.1 Overview 25
3.2 Quarter wavelength absorber 26
3.3 Micromesh Absorber 28
3.4 Material selection and Fabrication 31
3.4.1. Substrate material 31
3.4.2. Web structure 31
3.4.3. Sensor material 32
3.5 Conclusion 35
4 SIMULATION OF THERMAL TRANSIENTS 36
4.1 Overview 36
4.2 Study of variation of the thickness of the web-structure 40
4.3 Thermal Conductance G_{th} calculation 43
4.4 Characteristics of the device 45
4.4.1. Voltage responsivity vs. Frequency 45
4.4.2. Detectivity Vs frequency 47
4.5 Antenna Analysis 49
4.6 Microstrip Patch Antenna overview 49
4.7 Feed Techniques 50
4.8 Conclusion 55
5 CONCLUSIONS AND FUTURE WORK 56
REFERENCES 58
BIOGRAPHICAL INFORMATION 63

LIST OF ILLUSTRATIONS

Figure Page

1.1 Electromagnetic Spectrum 1

1.2 Infrared detection system 2

1.3 Classification of IR detectors 5

1.4 Model of a Photo-detector 6

2.1 Working of a pyroelectric sensor 14

2.2 Thin-film pyroelectric sensor 16

2.3 Thermal process of a Pyroelectric sensor 16

2.4 Output Circuit 1 18

2.5 Output Circuit 2 18

2.6 Equivalent circuit of a pyroelectric detector 19

3.1 Quarter wavelength absorber structure for 8-14 μm infrared radiation 26

3.2 Quarter wavelength absorber structure with the proposed dimensions 28

3.3 A simple web structure with two supporting legs connected to the substrate 29

3.4 Sol-gel preparation of PCT thin film [42] 33

3.5 Cross-section of the proposed pyroelectric infrared sensor 34

4.1 Mesh sensitivity analysis 37

4.2 Material Definition of Silicon Nitride in Coventorware 38

4.3 The 3-D model of the proposed Pyroelectric Detector 39

4.4 Spider web structure view with the sensor and the quarter wavelength absorber 39

4.5 Dimensions of the proposed pyroelectric detector 40

4.6 Sensor temperatures vs. time (Transient analysis) 44

4.7 Voltage responsivity (vs.) Frequency 46

4.8 Detectivity (vs.) Frequency.....47

4.9 Noise due to thermal conductance.....48

4.10 Johnson noise 48

4.11 Noise equivalent power.....49

4.12 a) Microstrip line feed, b) Coaxial line feed c) Proximity coupled feed 51

4.13 Antenna layout design.....52

4.14 S-parameter graph 53

4.15 Radiation patterns 53

4.16 Directivity graph.....54

LIST OF TABLES

Table Page

1.1 Comparison of principle types of uncooled thermal detectors 11

3.1 Dimensions of Spider web absorbers 30

3.2 Properties of silicon nitride 32

4.1 Dimensions of the proposed device 40

4.2 Thermal conductance in comparison with the radius of the web 41

4.3 Thickness of the web structure = 0.1μm 42

4.4 Thickness of the web = 0.3μm 42

4.5 Thickness of the web structure = 0.5μm 43

4.6 Thickness of the web structure =1μm 43

CHAPTER 1

INTRODUCTION

1.1 Overview

Electromagnetic radiation has electrical and magnetic components. Electromagnetic waves are produced by the motion of electrically charged particles. These waves are also called "electromagnetic radiation" (EM) because they radiate energy in the form of photons. They have the ability to travel through empty space, through air and other materials. Electromagnetic radiation is classified into several types according to the wavelength of the wave as radio waves, microwaves, infrared radiation, visible light, ultraviolet radiation, X-rays and gamma rays. A photon is the basic "unit" of all forms of electromagnetic radiation. EM radiation carries energy and momentum that may be imparted to matter with which it interacts.

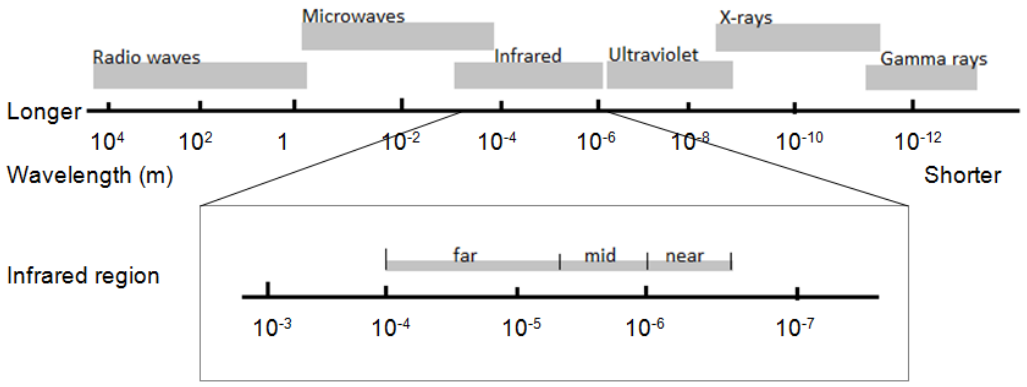

Figure 1.1 Electromagnetic Spectrum

1.2 Infrared Radiation

Electromagnetic waves lying in the wavelength region longer than the visible light wavelength, (i.e) from 0.75μm to 1000μm are called infrared radiation. The infrared region of the electromagnetic spectrum is divided into 3 regions,

i. Near Infrared region 0.7-3μm

ii. Mid-Infrared region 3-6μm

iii. Far Infrared region 8-15μm

Infrared radiation has the following characteristics,

a) *Invisible to human eye:* They can be used in night vision, security applications and to create visibility through fog or smoke.

b) *Small energy:* Infrared waves have small energy which is equal to the rotational and vibrational energy of molecules.

c) *Long wavelength:* Longer than visible region wavelength

d) Emitted from all objects.

An infrared detection system is shown below,

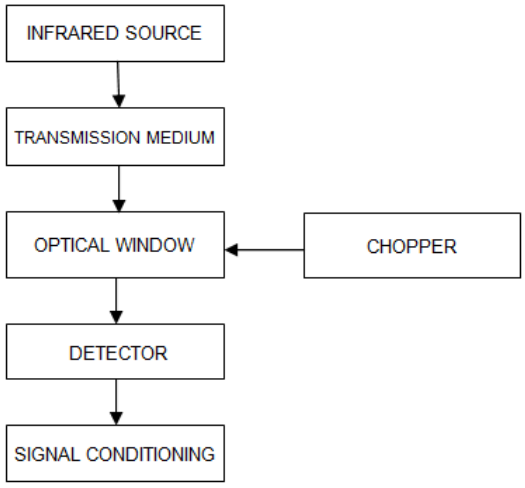

Figure 1.2 Infrared detection system

Any object that is above the absolute temperature 0 K is considered to emit infrared radiation. For the purpose of testing there are many sources of infrared radiation like the infrared bulb, globar, electric heater, mercury lamp, etc. Infrared detectors in general can be broadly classified into two groups: photon detectors and thermal detectors. The sensitivity of photon detectors is determined by the energy band gap of the semiconductor material utilized to sense the temperature change. These detectors require an external cooling mechanism to maintain the devices at a particular temperature for efficient operation, which significantly

increases the cost and complexity of the final IR sensor or imagery systems. In contrast, thermal IR detectors often operate near room temperature and usually do not require cryogenic cooling. This makes thermal IR imagers less costly and, thus attractive for various military and civilian applications.

1.3 Application of IR detectors

IR detection is widely used in the fields of manufacturing, agriculture, medicine, and astronomy. Given below are a few applications of infrared detectors,

1) Radiation Thermometers (RTs)

Radiation Thermometers are non-contact temperature sensors that measure temperature from the amount of thermal electromagnetic radiation received from a spot on the object under investigation. Radiation thermometers are available as point and array devices. The array type radiation thermometers are used to plot temperature distributions in the given area. The resulting image can be viewed as a 2-D temperature map of the area under inspection. They are used mainly in manufacturing process of metals, semiconductors, plastics, etc. Radiation thermometers enable automation and feedback control, as the thermal image of the product is analyzed for any faults and cracks as it comes out of the molding furnace and if the product found faulty it will be rejected from the conveyer. These devices are being used by fire fighters to improve their visibility during fire. One such radiation thermometer for near room temperature is discussed in [1] using HgCdTe as the sensor material.

2) Fire detectors

Infrared fire detectors work within the infrared spectral band. Hot gases that are a byproduct of the fire emit a specific spectral pattern in the infrared region, which can be sensed with a type of camera called a thermal imaging camera. The response time of this type of detector should be really low for better efficiency of the device for this application. Ultraviolet-infrared detectors respond to flaming fires emitting light in both the ultraviolet and infrared portion of the light spectrum. UV-IR detectors use both the ultraviolet and the infrared sensor to alarm simultaneously. This makes them very efficient in detecting the fire and resistant from

false alarms including candle lights, welding arc, stove burner, etc. Infrared sensors are also used for remote forest fires detection systems [2] because of the high amount of IR radiation emission of the combustion gases. PbSe has been identified as the ideal candidate for this application with a detectivity > 10^8 cm Hz ^{½} /W [2].

3) Fourier transform infrared spectroscopy:

Fourier transform infrared spectroscopy (FTIR) is a technique which is used to obtain an infrared spectrum of absorption, emission, photoconductivity of a solid, liquid or gas. The output gives the molecular finger print of the sample. GC-IR (gas chromatography-infrared spectrometry) is one of the applications of FTIR. A gas chromatograph can be used to separate the components of a mixture. The fractions containing single components are directed into an FTIR spectrometer, to provide the infrared spectrum of the sample. The GC-IR method is particularly useful for identifying isomers, which by their nature have identical masses. GC-FTIR has also been used to detect microbial degradation of pollutants like methane [3]. FTIR can also be used to measure the epitaxial layer thickness in a rapid and accurate way (Wolf and Tauber, 1986)

4) Thermal imaging and human body detection:

Thermal imaging and human body detection uses radiation thermometers to measure temperature at many points on a relatively large area and display a thermogram. Thermal imaging cameras detect radiation in the 9-14μm region of the infrared spectrum. As the temperature of an object increases the radiation emitted by that object increases correspondingly. This type of thermography is particularly used for military and security applications. Recently, airport personnel all around the world used thermography to detect suspected swine flu cases. The thermal profile of brain tumors and the surrounding cerebral cortex can be mapped with current technology using Infrared cameras [4]. Thermography is used in many industries to inspect the thermal insulation in structures and the leakage of heat from a structure.

1.4 Selection of IR detectors

The three main factors that influence the choice of an IR detector are the noise characteristics, detectivity, and the spectral response. These main characteristics are influenced by the absorption mechanisms, detector material, IR window, and the chopping frequency. Thermal detectors have a wide spectral response when compared to photon detectors, and so when choosing a photon detector it is advised to choose a detector which has a good response as close to the spectral band being used. Depending on the application of the detector the response time is also considered as an important factor for selection of a particular IR detector. Other than the above mentioned factors, robustness, cost of fabrication, ease of use, and packaging also play a secondary role in the selection of an IR detector. Typically a detector which works in room temperature will reduce the cost of the detection system as a whole as it avoids the use of cryogenic cooling system.

1.5 Types of IR detectors

The different types of thermal and photo detectors are shown below,

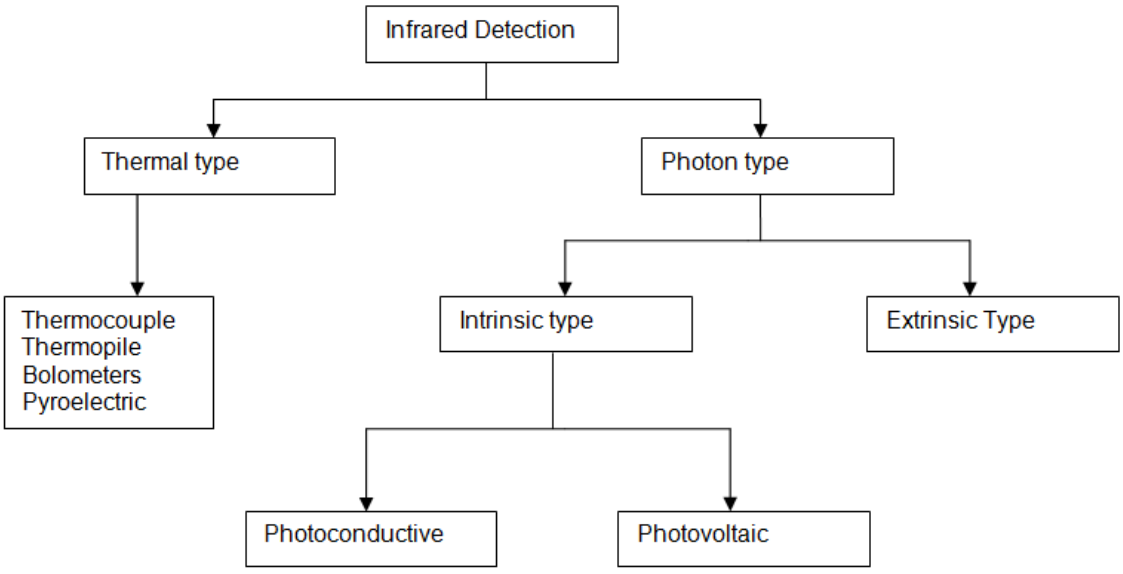

Figure 1.3 Classification of IR detectors

1.6 Photon detectors

In photon detectors, the photons (basic part of the electromagnetic wave) are absorbed by the semiconductor material, which generates free charge carriers. These free charge carriers are measured as a current across the diode. This is the working mechanism of the photon based Infrared detection. The first generation of infrared photon detectors were mostly used as scanning systems, the second generation photon infrared systems was used as staring systems, and the third generation of IR systems concentrates on improving the thermal resolution, frame rates, and multicolor capability [5]. One of the most important materials used to construct an IR photon detection system is HgCdTe. Mercury cadmium telluride is used to construct IRFPA's on a large scale. ([6] J.Bajaj, Rockwell science center, 1999) have fabricated a hybrid IRFPA which has a spectral region from 1-16μm. HgCdTe has been considered as one of the materials for Infrared radiation detection from 1958 [7]. One of the major disadvantages of Mercury cadmium telluride is its fabrication as Hg has a high vapor pressure. PbSnTe was a material that was developed in parallel with HgCdTe as a successor but due to a large coefficient of thermal expansion with silicon and high dielectric constant its use was reduced [8].

The incident of infrared radiation on the semiconductor material causes the detector properties like resistance, voltage and current to change.

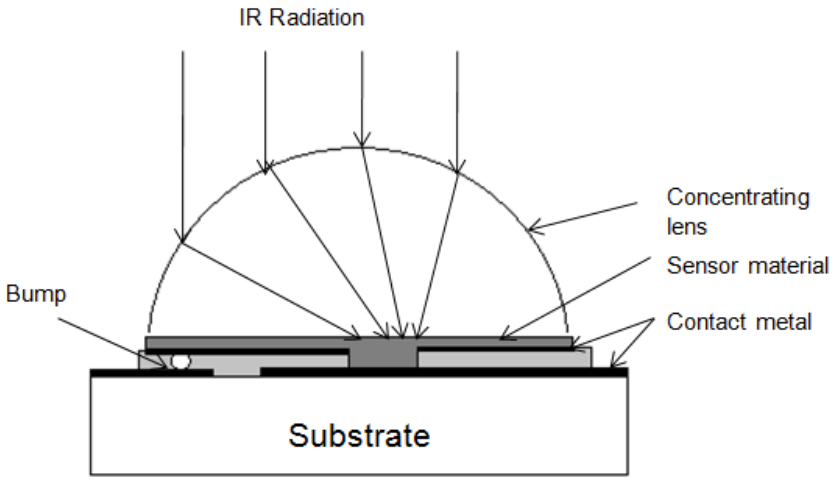

Figure 1.4 Model of a Photo-detector

The current responsivity of the photo detector is determined by the quantum efficiency and the photoelectric gain, G. The quantum efficiency describes how well the detector is coupled to the incoming IR radiation [8]. Both the values are assumed here as constant over the volume of the device. The energy of a photon is related to its wavelength by the formula,

$$E = hc/\lambda \tag{1.1}$$

where h is the Planck constant = 6.6×10^{-34} J-s, c is the speed of light = 3×10^{8} m/s and λ is the wavelength. The spectral current responsivity is equal to,

$$R_i = \frac{\lambda \eta}{hc} qg \tag{1.2}$$

where λ is the wavelength, h is the plank's constant, c is the light velocity, q is the electron charge and g is the photoelectric current gain [9]. The electromagnetic energy is transferred to an electron which in turn excites the electron, so that the electron gains sufficient amount of energy to cross the band gap region of the semiconductor and become a free electron. The cooling requirements remain as the main obstacle in the widespread use of photon detectors for infrared radiation. Most detectors need to be operated at very low temperatures. Recently a great amount of research has been done in uncooled photon detectors. Different ways to improve the performance of photon detectors without cooling have been developed [10].

1.7 Thermal Detectors

There are three ways in which heat is transferred from one body to the other; they are by conduction, convection and radiation. Infrared detectors use radiation as the method of heat transfer from the electromagnetic waves to the sensor. Thermal infrared detectors are usually designed to operate in the 3 – 15μm wavelength region of the electromagnetic spectrum. The thermal detectors are classified by the way in which the temperature change is measured by the sensor. They are thermoresistive, thermocouples, piezoelectric and pyroelectric

There are three basic principles of operation of a thermal detector. They are,

1. A non-thermal signal is converted into heat flow.

2. The heat flow is converted into the thermal signal domain by the change in temperature of the absorbing material
3. The temperature change is transduced into an electrical signal by the temperature sensor

Kirchhoff's law states that "*If radiation is incident on a surface, the sum of the absorbed, reflected and transmitted radiation is equal to the total incident radiation, for each wavelength*" [11]. The fraction of radiation that is absorbed is responsible for the temperature raise of the sensor material. The amount of absorption is defined by absorptivity (α) of the sensor. The thermal capacity of a thermal sensor is an important factor. It is defined as the heat necessary to increase the temperature of a given system by 1K and equals the mass of the system m times the specific heat, c_p, $C_{th} = c_p m$ [11]. A body that absorbs all the radiation falling on it and a body whose emissivity at the surface is equal to 1 is called a blackbody. The Stefan Boltzmann law states that "The power emitted by a gray or black body is equal to

$$P(T) = \epsilon \sigma T^4 \tag{1.3}$$

where ϵ - emissivity at the surface and σ - Stefan Boltzmann constant = 56.7×10^{-9} $W/m^2 - K^4$ [11]

There are different kinds of thermal detectors based on the principle of operation.

Thermopiles: Among the First generation of thermopiles were metal-metal junctions consisting of copper-constantan and manganin-constantan junctions. These were found to be highly robust and highly reproducible detectors which can be used for investigation therapeutic effects of hypothermia [12]. Different metal were considered to improve the sensitivity of thermopiles. Silicon micromachining techniques have helped improve the sensitivity of the thermopile structures. Lahji et al fabricated a thermopile in which bismuth-antimony pairs were evaporated into a thin silicon membrane insulated with CVD oxide. In the later designs silicon was also made an active part of the thermopile sensor. Van Herwaardeen et al fabricated a thermopile in which p-type conducting strips were diffused in an n-type epitaxial layer. Aluminum contacts were then used to connect the p-type regions. Silver-bismuth junctions were found to have higher sensitivity [15]. Semiconductor elements have proven to offer better sensitivity than using

metal couples. Modern fabrication techniques like photolithography and vacuum deposition have improved the efficiency of thermopiles to a large extent. The choice of substrate for deposition depends on the application. These micromachining techniques have made possible the development of small area high detectivity thermopiles. Usually sufficient isolation is designed from the sensor to the substrate. The metals usually used are antimony and bismuth since these have good thermoelectric properties, but silver-bismuth is also used. Thermopiles constructed this way can have response time less than 30 ns and can be used as heterodyne detectors

Bolometer: A bolometer works on the principle of measurement of change in resistance corresponding to the change in temperature. The resistance sensor is placed below a heat absorbing material and on an isolated surface. Both metal film and thermister (change in resistance based on change in temperature) bolometers have been in use. Semiconductor bolometers which are externally cooled are being used in space applications for their high sensitivity and detectivity. Recently attempts have been made to develop bolometers by using newer materials with larger temperature coefficients. A promising material is the semiconducting lanthanum-doped barium strontium titanate [29]. Liquid helium cooled bolometers are still employed in far infrared spectroscopy and astronomy where the performance of the uncooled detectors is inadequate. The selection of the optimum material for constructing this type of bolometer is very critical.

A detailed study of the Ge bolometer was done in the recent past. The performance of these bolometers improves since the temperature is reduced below 4K. The simplest procedure is to pump the helium to reduce the operating temperature. In this way an operating temperature between 1K and 2K can be obtained, but (Drew and Sievers, 1969 [27]) have described a Helium cryostat operating at about 0.3K. Micromachining techniques are employed to obtain the isolation of the sensor from the substrate. A bias current is needed to calibrate the device and to set a reference point for measurement of the change in resistance. A high temperature coefficient of resistance (TCR) and a small 1/f noise are desirable material

properties for a perfect bolometer. At the same time, it must be possible to integrate the temperature sensing material together with signal read-out electronics (e.g. a CMOS wafer) in a cost efficient way. Today, the most common bolometer temperature sensing materials are vanadium alloy oxide layer [17], metal bolometers on porous silicon (Si) [18] and ceramic bolometers [19].

Pyroelectric Detector: Considerable amount of work has been made in the development of pyroelectric detectors by Putley 1971, Hadni 1971. It has been noted that for most purposes, from the past decades triglycine sulphate (TGS) or its derivatives are the most suitable materials for pyroelectric detection. Other pyroelectric materials such as strontium barium niobate (SBN) (Glass and Abrams 1971), lithium sulphate and members of the lead zirconate titanate family (Mahler et al 1972, Yamaka et al 1972 [27]) may be more suitable for some specific applications. The optimum choice of material properties has been discussed in detail by Putley (1970) [27]. The most relevant material properties for an efficient pyroelectric sensor material are the pyroelectric coefficient, the dielectric constant and the thermal capacity. In a desirable material the pyroelectric coefficient should be large, both components of the dielectric constant small and the thermal capacity small. TGS does not possess the largest known pyroelectric coefficient at room temperature. Higher values being found in BST [20] and in some doped lead zirconate titanate ceramics, but the materials with larger pyroelectric coefficients have much larger dielectric constants with large loss factors. In the best pyroelectric detectors the dominant source of noise is the Johnson noise associated with the dielectric loss, followed by the amplifier noise. The capacity of a small TGS detector could fall so low that it could become less than the amplifier input capacity. Detectors made from these materials are somewhat more robust than TGS, although this advantage has been exaggerated, and they are being produced to meet requirements for simple cheap detectors for applications not requiring the highest performance. The improvement in the performance of TGS detectors has been brought about by improvements in the quality of TGS and of the performance of the associated

high input impedance low noise amplifier. These results indicate the pyroelectric detector amongst the best uncooled thermal detectors. The attractions of using a pyroelectric detector in this way are that it operates at room temperature and it has a very high voltage responsivity and detectivity.

Table 1.1 Comparison of principle types of uncooled thermal detectors

Parameter	**Monolithic bolometer**	**Monolithic pyroelectric detector**	**Monolithic thermoelectric detector**	**Hybrid pyroelectric detector**
Responsivity	High	High	Low	High
Bias required	Yes	No	No	No
Chopper required	No	Yes	No	Yes
FPA	Yes	No	Yes	No
Possibility of performance improvement	High	High	Medium	Low

In recent times, hybrid FPA's have replaced point detectors. With the advancement in MEMS fabrication technologies, it is possible to produce uncooled pyroelectric infrared detectors with a very good absorber design. The reductions of the size devices have stated reaching saturation point and 3-D stacked devices have started emerging. The read out electronics in pyroelectric detectors have started to be integrated under the sensor using a solder ball. The height of the solder ball gives the necessary isolation between the sensor and the substrate Even though these methods are still under research; they prove that IR detectors with very high sensitivity and responsivity could be manufactured in micro scale in the near future.

1.8 Motivation and Goals

Spider-web absorber designs in absorbers started with the research by J.J block et al [21] about a novel bolometer design for mm-wave astrophysics. They had proposed a spiderweb absorber design that yielded better absorption. Later F.B liewiett et al. 1999 [37] proposed the fabrication and characterization of infrared and sub-mm spiderweb bolometers with low T_c superconducting transition edge thermometers. Thereafter a lot of designs involving absorber designs shaped like a mesh of lossy wires have been under consideration as they have very high absorptivity. M.J.M.E de Nivelle et al proposed a high T_c bolometer with silicon nitride web structure. This device had a very high detectivity in the order of $5.4x10^{10}$ cm $\sqrt{Hz}/W$. a number of these structures were used with bolometers for infrared detection. This aspect can be used to inspect the use of pyroelectric sensors combined with these absorbers which could yield in very high detectivity. L.N.Hadley and D.M.Dennison proposed a novel quarter wavelength absorber design in their two part journal [22], [23] in 1947. The design consists of three layers. The metal film on top is impedance matched to free space, so that 50% of the incident radiation is absorbed and 50% is transmitted. The second layer is a dielectric layer, and the third layer is a total reflection layer which reflects back the transmitted radiation. The radiation destructively interferes in the middle layer yielding more than 95% absorption easily. One such absorber design is proposed in this design. These absorber designs, if implemented, could result in very high absorption. When these absorbers are combined with highly effective pyroelectric sensors, the result is very high sensitivity and detectivity at room temperatures.

PCT (Lead calcium Titanate) is one of the newest and the most efficient pyroelectric sensors that have been under consideration for the development of long wavelength pyrodetectors recently. Sonalee Chopra et al, 2003 [24] have done extensive research in analyzing the material properties of PCT thin films. The pyroelectric coefficient and figure of merit of PCT thin films was found to be $43x10^{-9}$ C cm^{-2} K^{-1} and 2340 V $cm^{-2}J^{-1}$ [24]. An efficient design of an infrared detector involves a good design of the infrared absorber, a good isolation from the substrate, an efficient type of detection mechanism, an efficient type of sensor

material, easy to fabricate, have a good detectivity and voltage response and have good isolation from the background thermal noise. Thus the main objectives of this thesis is to design an infrared detector,

- That has an efficient detection mechanism
- That has a high absorptivity
- That has a high voltage response
- That has a high detectivity
- That has high figures of merit
- That has very low thermal conductivity between the sensor and the substrate

Keeping all these points in mind a new type of infrared detector has been proposed here. Coventorware was used to create the mask designs and the 3-D models of the device.

1.9 Organization of the Document

Chapter 2 provides a general introduction to pyroelectricity, the physics behind the operation of pyroelectric detectors. It describes the various noise sources and the noise parameters that affect the pyroelectric detector.

Chapter 3 describes the absorber design and the effects of the structure of the absorber on the sensor material are explained. Various other parameters that affect the output of the detector are discussed. It also provides suggestions on various fabrication techniques that can be employed to fabricate the sensor and the absorption structure.

Chapter 4 includes all the simulation data and the results based on the simulation run in Coventorware and ADS-Genesys. The mask design was created and the 3-D model simulated, meshed and thermal transient analysis was performed on the device.

Chapter 5 concludes the work and also discusses future research that, if executed, could increase the efficiency of the proposed sensor.

CHAPTER 2

PYROELECTRICITY

2.1 Overview

Pyroelectricity can be defined as the temperature dependence of the spontaneous polarization of certain solids which may be either single crystals or poly crystalline materials. If the temperature of the material is raised by a small amount, the electrical polarization of the material is changed and a current can be measured from certain faces of the crystal or between certain faces of the disk.

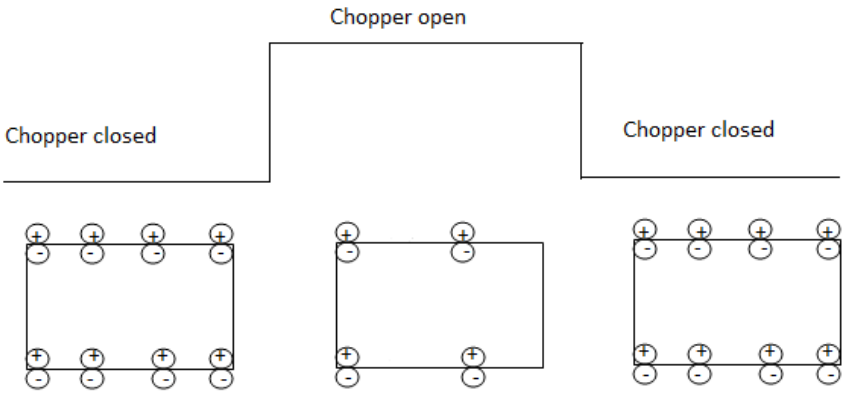

Figure 2.1 Working of a pyroelectric sensor

In order for a material to be pyroelectric, each fundamental unit of the material must have an electric dipole. If the dipoles throughout the material are aligned in such a way that the self-cancellation does not occur then the material will exhibit an electrical polarization called spontaneous polarization [25]. If the material is maintained in a constant temperature, the internal spontaneous polarization is masked by the accumulation of charges on the external surface, if the material undergoes a change in temperature (chopper ON and OFF as shown in the diagram), the strength of the dipoles changes, causing the surface charges to redistribute

themselves. This effect can be measured by connecting an ammeter between conductive electrodes placed on the appropriate surfaces of the substance. This effect is called pyroelectric effect.

A simple pyroelectric detector consists of a pyroelectric element with metal electrodes on its opposite faces. Generally ferroelectric materials are best suited for pyroelectric detectors [26]. They have large number of different domains with different direction of polarization, such that the net effect is zero. Usually poling is done to orient these domains parallel to each other. Even across a perfectly poled detector, no observable voltage is found, because its internal polarization is balanced by a surface charge which accumulates via various leakage paths between the two faces. For this reason the pyroelectric detector can only be used to detect a modulating signal. When the detector is heated by a source, electromagnetic radiation is this case, the polarization changes by an amount that is determined by the temperature change and pyroelectric coefficient of the material. Thus the charge measured across the capacitor formed by the two metal electrodes is directly linked to the polarization caused by the heat flux that occurs in the detector.

The basic operating principle is governed by the formula

$$\Delta Q = Ap\Delta T \tag{2.1}$$

where, A is the area of the capacitor and p is the pyroelectric coefficient and ΔT is the change in temperature. The heat transfer process is well described in the figure 2.3. The heat sink can be compared to the silicon substrate and the power input is the infrared light.

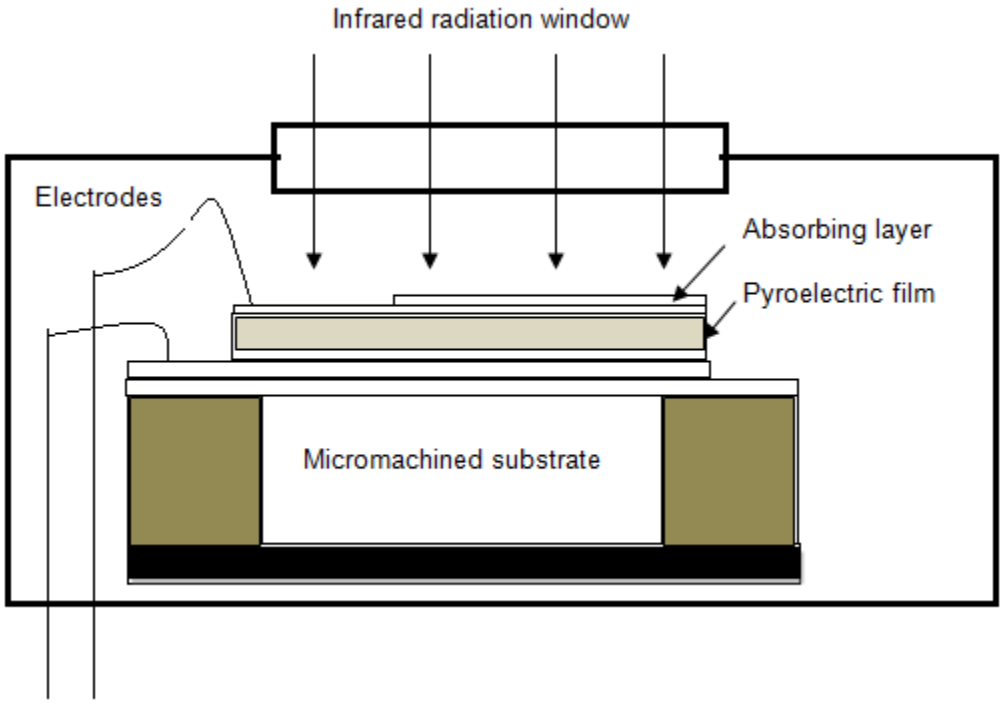

Figure 2.2 Thin-film pyroelectric sensor

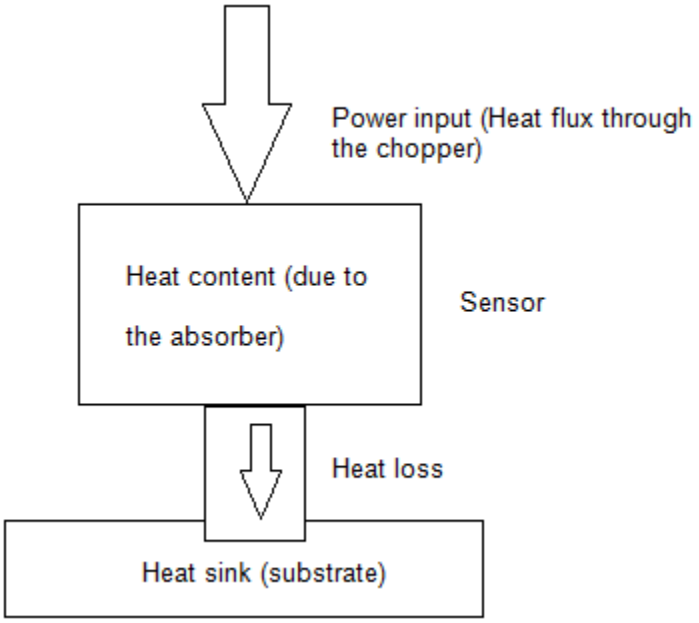

Figure 2.3 Thermal process of a Pyroelectric sensor

The detector is represented by a thermal capacitance C_{th} coupled via a thermal conductance G_{th} to a heat sink which is maintained at a constant temperature T. In the absence of the radiation input the average temperature of the detector will also be T. When a modulating

radiation input infrared signal is given to the detector, the rise in temperature is found by solving the heat balance equation, [8]

$$C_{th}\frac{d\Delta T}{dt} + G_{th}\,\Delta T = \epsilon\Phi \tag{2.2}$$

where, ΔT is the temperature difference due to optical signalΦ, between the detector and its surroundings, and ε is the emissivity of the detector. Assuming the radiant power to be a periodic function, the change in temperature of any thermal detector due to incident radiant flux is given by, [9]

$$\Delta T = \frac{\varepsilon\Phi_0}{(\,G_{th} + \,\omega^2 C_{th}^2\,)^{1/2}} \tag{2.3}$$

It is advantageous to make ΔT as large as possible. Thermal capacity of the detector and its thermal conductivity to the heat sink must be made as small as possible. The heat capacity of the detector must also be small to improve the sensitivity. This means that a smaller detector smaller connecting wires to the heat sink are desired. A characteristics thermal response time constant for the detector can therefore be defined as, [9]

$$\tau_{th} = \frac{C_{th}}{G_{th}} = \,C_{th}R_{th} \tag{2.4}$$

where R_{th} is the thermal resistance. Then the equation can be written as

$$\Delta T = \frac{\varepsilon\Phi_0 R_{th}}{(1+\omega^2\tau_{th}^2)^{1/2}} \tag{2.5}$$

In order to detect these very small charges, a low noise high impedance amplifier is necessary. A source follower configuration is shown below,

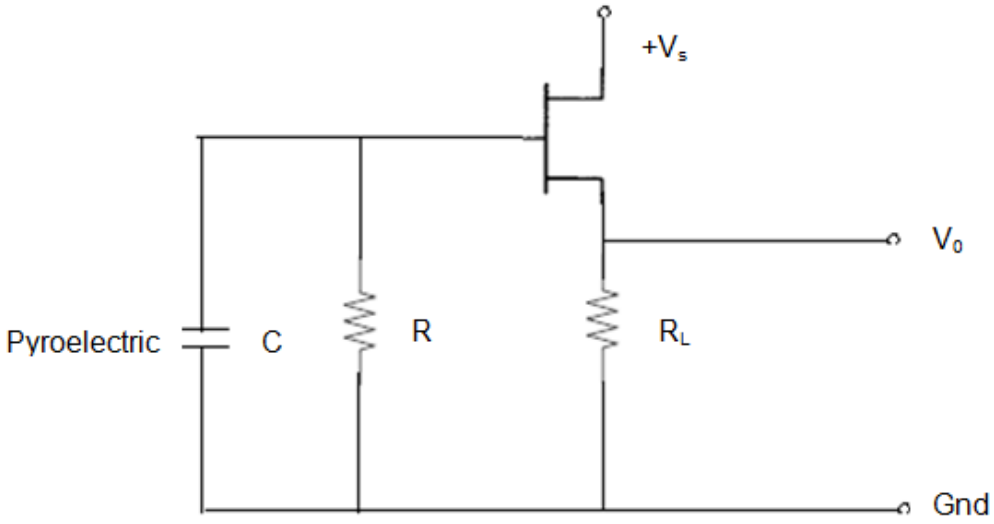

Figure 2.4 Output Circuit 1

If the bias resistor R is sufficiently high, the output voltage V_0 corresponds to the voltage generated in the pyroelectric element. For this to be true the value of R must be in the range of 10^{10} Ohms. If R is small then the V_0 is proportional to the current generated by the detector and flowing through R. An alternative arrangement using an op-amp is also shown.

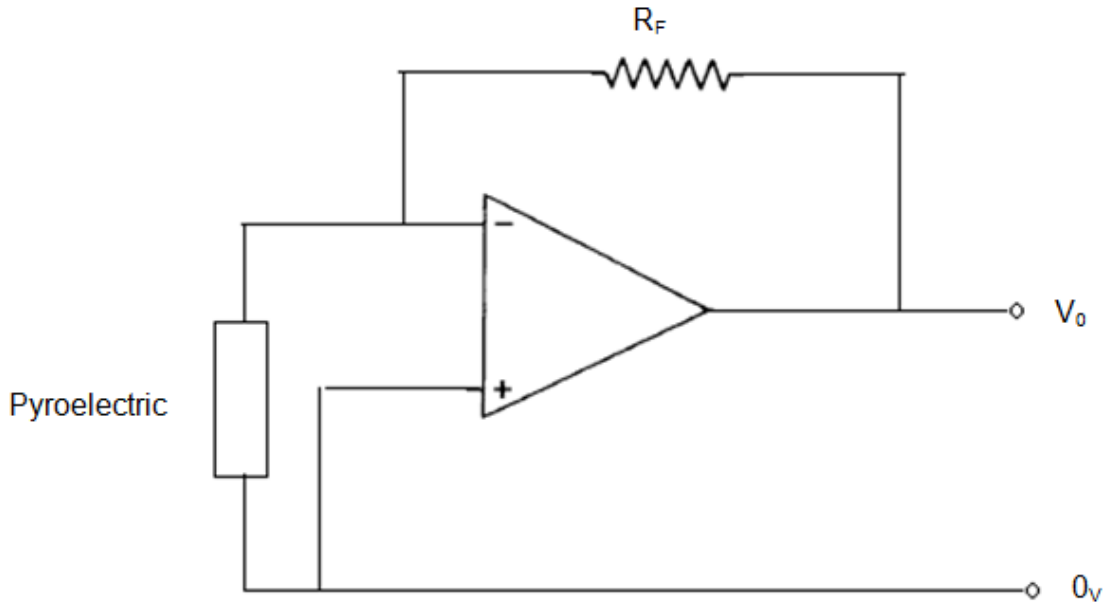

Figure 2.5 Output Circuit 2

There are many other noise parameters that set the detection limit for the detector. The largest pyroelectric effects are observed in a class of materials called ferroelectrics. The usefulness of a detector can be usually assessed in terms of the minimum detectable incident power. This can be represented as a function of both the responsivity and the noise generated in the detector and its amplifier electronics. The simple circuitry associated with the pyroelectric detector makes it a suitable candidate for hybrid designs. Hybrid designs are the combination of a CMOS and MEMS process to fabricate the read out electronics under the sensor.

2.2 Voltage Responsivity

A more explanatory equivalent circuit of a pyroelectric detector is shown below,

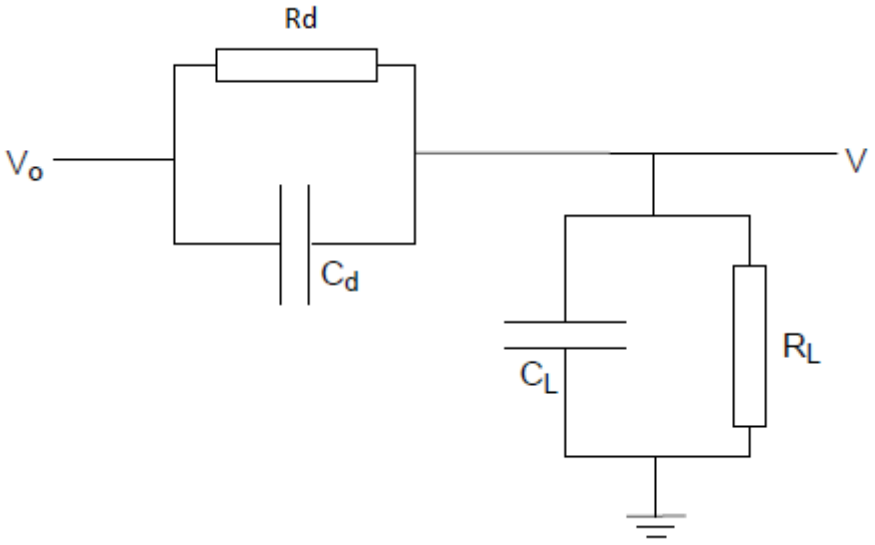

Figure 2.6 Equivalent circuit of a pyroelectric detector

R_d – Resistance of the detector, C_d –capacitance of the detector, C_L –capacitance of the load, R_L – capacitance of the load, V_0 – applied bias

Consider the case of a stationary sinusoidally modulated radiation power, $W = We^{i\omega t}$, yielding a temperature modulation amplitude of [28]

$$|\theta_\omega| = \frac{\eta W_\omega}{G\sqrt{1+\omega^2\tau_{th}^2}} \tag{2.6}$$

The current responsivity is the current per watt of radiation power falling onto the detector element, [28]

$$R_j(\omega) = \frac{J_\omega}{W_\omega} = \frac{p\eta\omega \mathrm{A}}{G\sqrt{1+\omega^2\tau_{th}^2}} \tag{2.7}$$

where, $J_\omega = pA\omega|\theta_\omega|$. The electrical time constant $\tau_{el} = Rp * C$. The voltage responsivity is given by [28]

$$R_v(\omega) = |Z(\omega)|\, R_j(\omega) = \frac{p\eta\omega A R_p}{G\sqrt{1+\omega^2\tau_{th}^2}\sqrt{1+\omega^2\tau_{el}^2}} \tag{2.8}$$

The choice of pyroelectric material depends on a number of parameters like the size of material, frequency of operation and the operating temperature. It is possible to determine a number of figures-of-merit, which describes the contribution of the physical properties of the material to the performance of the device. The figure of merit of voltage responsivity of thin film device is given by, [26]

$$F_v = \frac{p}{\varepsilon_0 \varepsilon_r} \tag{2.9}$$

where ε_r is the relative permeability of the material.

2.3 Noise Mechanisms

The minimum detectable signal from a pyroelectric detector is limited by various noise sources in the detector element, the load resistors and capacitors and the external current measuring circuit. The noise voltage is usually expressed in V/√Hz .These noise sources are,

1) *Temperature or radiation noise:* The thermodynamic fluctuations in the temperature of the detector element due to radiative exchange of heat with the background or conductive exchange of heat with the heat sink produces a signal voltage. This is given by [29],

$$\Delta V_t = R_v \frac{\sqrt{4KT^2 G_{th}}}{\eta} \tag{2.10}$$

2) *Johnson noise:* Johnson noise arises from the random thermal motion of charge carriers in the pyroelectric element. Practically a pyroelectric material is not a perfect capacitor. The

leakage capacitance and the dielectric constant are the major factors contributing to the Johnson noise of the detector. This is given by [29],

$$\Delta V_j = \frac{\sqrt{4KTR_{tot}}}{\sqrt{1+\omega^2\tau_\varepsilon^2}} \tag{2.11}$$

In this expression R_{tot} represents the total equivalent resistance of both the sensing element and the external circuit.

3) *Amplifier noises:* there are two types of amplifier noises. They are amplifier current noise given by [29],

$$\Delta V_i = \frac{\Delta i_A R_{\omega t}}{\sqrt{1+\ \omega^2\tau_e^2}} \tag{2.12}$$

and amplifier voltage noise V_a. They can be obtained from the manufacturer. The total noise voltage is obtained by summing all the noise values.

$$V_n^2 = V_t^2 + V_j^2 + V_i^2 + V_a^2 \tag{2.13}$$

2.4 Noise Equivalent Power

The sensitivity of a particular detector is usually expressed in terms of its noise equivalent power (NEP). It is defined as the incident power which is required to produce a signal equal to the rms value of the noise voltage, [26]

$$NEP = \frac{V_n}{R_v} \tag{2.14}$$

The unit of NEP is usually, $W/Hz^{1/2}$. It will be specified for a particular frequency. The detectivity of a sensor is given by the reciprocal of the Noise Equivalent Power. It is therefore given by the formula, [26]

$$D^* = \frac{A^{1/2}}{NEP} \tag{2.15}$$

The unit of detectivity is cm $Hz^{1/2}W^{-1}$.

Further degradation of the sensor output, sensitivity or detectivity can occur because of the following reasons,

1. Packaging of the detector (reflection and absorption losses)

2. Influence of electrical contacts, conduction through the supports
3. Additional noise sources

In simple terms, the figure of merit of detectivity of the pyroelectric detector is given by,

$$F_d = \frac{p}{C_{th}(\varepsilon_0 \varepsilon_r tan\delta)^{1/2}} \tag{2.16}$$

where tanδ is the loss tangent of the detector material [8]. The detectivity can be expressed in terms of the reciprocal of NEP as follows,

$$D^* = \frac{R_v \sqrt{\Delta f * A_d}}{V_n} \tag{2.17}$$

$$NEP = \frac{\Delta V_n}{R_v} \tag{2.18}$$

2.5 Other effects

Microphony

In certain applications pyroelectric detectors are prone to microphony. Microphony is the electrical output produced by the mechanical vibration in the device due to environmental factors. This type of noise becomes easily dominant form of noise. The main cause of this type of noise is the piezoelectric nature of pyroelectric materials. Microphony effects are reduced by mounting the detector on point contacts or a less rigid structure. [26]

Thermally Induced Transients

A Pyroelectric detector, if subjected to fast changes in ambient temperature fast pulses are observed, superimposed in normal pyroelectric response. These noise pulses are called thermally induced transients [26].

Thermal mismatch during processing

Pyroelectric thin films are grown usually in the temperature range 500-700°C. The para-to-ferroelectric phase transition occurs when cooling from the growth temperature [28]. Usually the mismatch in thermal expansion between the sensor and the substrate causes a variation in the c-axis orientation.

2.6 Modes of Operation

The pyroelectric detector operates in two modes of operation they are the current mode and the voltage mode. In the voltage mode, the pyroelectric current charges the pyroelectric element capacitor, and the resulting voltage is measured by a source follower circuit. At common modulation frequencies between 1-10 Hz voltage mode detectors operate beyond the thermal and electric time constant in 1/f behavior, typical signals are a few mV. In current mode the pyroelectric current is transformed by a current-voltage-converter (basically on OpAmp with feedback components, also called a transimpedance-amplifier TIA). Current mode detectors normally operate between the thermal and the electrical time constant, at frequencies from 1Hz up to 1 kHz, with typical signals about 100 mV or more. For the detector performance the frequency response defined by thermal and electrical time constant and the resulting signal is of key importance. The thermal time constant is a measure of the thermal coupling of the pyroelectric element to the environment is effective in both operation modes. The electrical time constant in voltage mode is defined as the product of the pyroelectric material capacitance and the gate resistor and can be changed only in a small range. In current mode it is defined as the product of feedback resistor and feedback capacitance. Additionally the achievable gain of the pyroelectrical signal in current mode is much higher and can be adjusted easily by changing the feedback resistor, while in voltage mode the gain is only around 0.8. Therefore in current mode the frequency response and signal voltage of the detector can be designed much more individually, which results in possible operation at high frequencies up to 1 kHz resulting in a very short response time [26].

2.7 Conclusions

In this chapter the definition of pyroelectricity and the physics behind pyroelectric detectors were discussed with corresponding equations. The operating principle and the heat balance equation were discussed in detail. It is found that perovskite materials are superior to other materials since it has better control over the properties of the materials. Various materials were considered as the sensor material for this project. Materials like PZT, Lithium tantalate,

and Strontium barium niobate can be used as the sensor material. However PCT Calcium Modified Lead titanate was chosen as the sensor material from the perovskite ferroelectric family. The reasons for choosing this material as the sensor material will be discussed in the next chapter. The voltage responsivity, detectivity and the noise parameters were discussed with corresponding equations. The qualitative pyroelectric measurements can be performed by

1) Static methods

2) Dynamic methods

   a) Pyroelectric current method

   b) Shunt resistor method

   c) Radiant heating method

   d) Charge integration capacitor method

3) Indirect methods

Based upon the materials and the properties discussed earlier appropriate methods are chosen to measure the output current.

CHAPTER 3

PYROELECTRIC SENSOR DESIGN

3.1 Overview

The proposed Infrared pyroelectric MEMS sensor achieves a really high voltage responsivity R_V and detectivity D, by using an efficient absorber design in combination with very low thermal conductivity to the substrate material. The absorber design is an important part of a thermal sensor. There are a lot of absorbers that have been used traditionally. Maximum absorption of heat can be obtained by having an absorbing layer deposited on the detector. There are two main requirements for the absorbing layer to have very high efficiency, they are, a) the absorber must be able to work at large range of wavelengths and b) it should have a low thermal mass. There are three main types of designs that have been used traditionally. They are,

1. The first class includes metal-black coatings that show significant absorption in the visible and near IR [30]. They have been widely used in the past on thermopiles, bolometers, and pyroelectric detectors. They have high thermal capacity and represent fragile absorber systems
2. In the second class included thin metal film absorbs. This absorber shows a quiet constant value over the whole IR, and that explains the wide use of such films as IR absorbers [31]. The third class of absorbers was quarter wavelength absorbers. L.N.Hadley and D.M.Dennison [22] [23] proposed this concept. This type of absorbers yielded upto 95% absorption of the incoming radiation

3. Even though maximum absorption could be obtained by the third class of detectors, the thermal capacity was still high. To overcome this problem a fourth class of absorbers were developed. They were a mesh of lossy wires. JJ.Bock et al, 1995 [21] proposed a spider web type absorber with an absorber coating on it. Hu Tao et al 2008 [19] proposed a metametal absorber for the terahertz regime which yielded an experimental absorptivity of 70%.

For this project two types of absorbers have been proposed from the class 3 and class 4 type absorbers.

3.2 Quarter wavelength absorber

A quarter-wavelength absorbance structure was designed and used here to have maximum absorption. The structure is shown below.

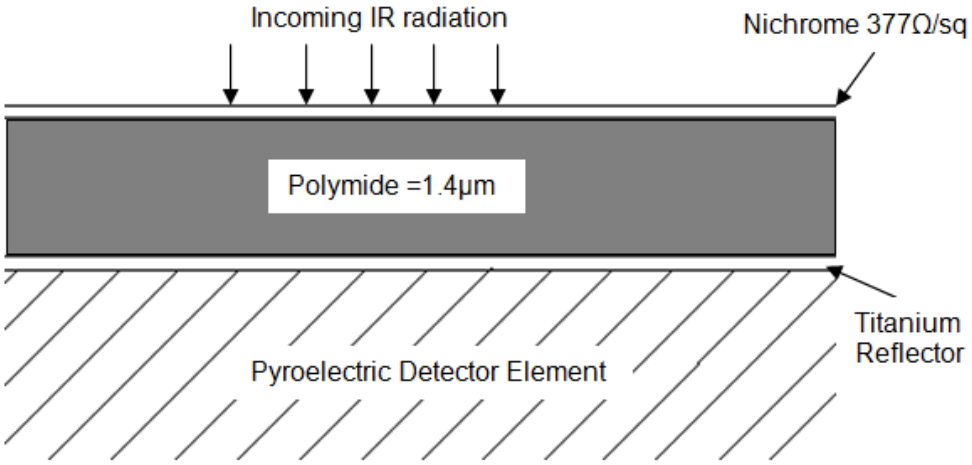

Figure 3.1 Quarter wavelength absorber structure for 8-14 μm infrared radiation

The metal films deposited at the top and bottom of the quarter wavelength structure. The top metal film which is exposed to the IR radiation is impedance matched to the free space i.e. the surface impedance of the top metal is 377Ω, so that approximately 50% of the incident radiation is absorbed and 50% is transmitted. The transmitted radiation goes through a quarter wavelength dielectric layer and is reflected by the lower metal film which has a very high reflectivity and destructively interferes, giving zero reflection and 100% absorption ideally [32].

There are three main requirements to design a perfect absorbing layer for a pyroelectric detector. They are,

a) The surface impedance of the metal absorbing layer needs to be equal to 377 Ω (matching the impedance of free space)

b) The thickness of the dielectric film Δ is determined from the relation [33]

$$\Delta = \frac{(2m+1)\lambda}{4n} \tag{3.1}$$

c) The bottom layer (reflecting layer) needs to have excellent reflection coefficient at the specified wavelength.

The theory of absorption from this structure has been well studied. Hadley and Dennison [22], [23], have discussed the reflection from a structure consisting of a thin metal film separated from a mirror like metal film dielectric. The same structure was considered by Silberg [34] and Heavens. Thus the absorption of an idealized structure can be expressed as, [35]

$$A = \frac{4f}{[(f+1)^2 + n^2 cot^2(2\Pi nd/\lambda)]} \tag{3.2}$$

where f= 377 / R_a, where R_a is the absorber layer sheet resistivity in Ω/sq, n is the refractive index of the dielectric layer, d is the thickness of the dielectric, and λ is the wavelength of the incident IR radiation. This equation assumes 100% reflection of the incident radiation by the metal reflector layer. For the proposed design the thickness of the quarter wavelength absorber is obtained from the above equation. The nichrome disc is kept at 0.2 μm thick so that the impedance match of 377Ω/sq is maintained. The thickness of the titanium reflector is usually in the nanometer (nm) range. The thickness of the dielectric is obtained by,

$$\mathrm{d} = \frac{\lambda}{4\mathrm{n}} = 1.11\mu\mathrm{m}\ (\ 8\mu\mathrm{m\ infrared\ wavelength\ is\ assumed})$$

The sheet resistance of nichrome is assumed to be 300Ω. With the calculated values of thickness it is found that the absorption could be as high as 97%. The structure of the quarter wavelength absorber is as shown below.

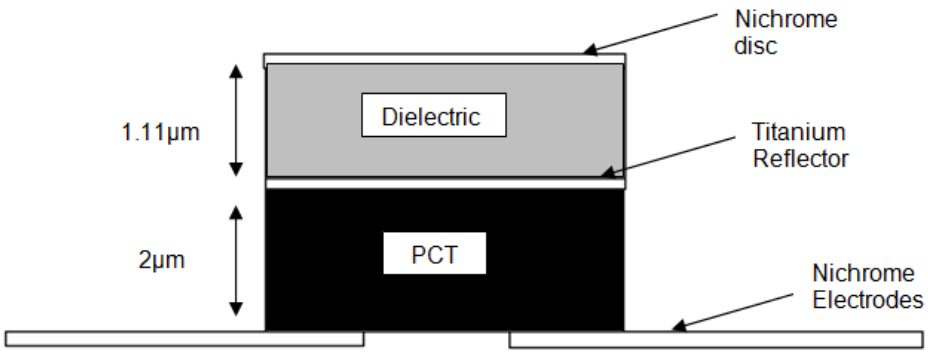

Figure 3.2 Quarter wavelength absorber structure with the proposed dimensions

3.3 Micromesh Absorber

An important part of all IR detector systems is the absorber efficiency that indicates how much heat falling on the surface of the detector is converted into transduced signal. Composite detectors traditionally use a uniform metallic film deposited on a dielectric substrate as a broadband absorber [36]. To obtain frequency independent absorption, its impedance of the dielectric film should match the impedance of free space, Z_0=377 Ω/sq. The conventional heat absorbers are deposited as a layer on top of the sensor material. This deposition results in a very high heat capacity of the overall structure. The high heat capacity is also a result of surface contamination of the substrate [36]. It is possible to achieve very high absorptivity by constructing a mesh of lossy wires, with a high absorbing coating on the mesh. One such construction was demonstrated by J.J. Bock et al [21]. Following them a lot of research has been carried out in this area. A lot of designs of the mesh of wires have been made possible by micromachining methods. Usually the mesh is formed by micromachining, and then the sensor is attached to the center of the mesh. Until now a number of bolometers have been constructed by this method and have resulted in high sensitivity designs. One such structure is shown in the figure 3.3,

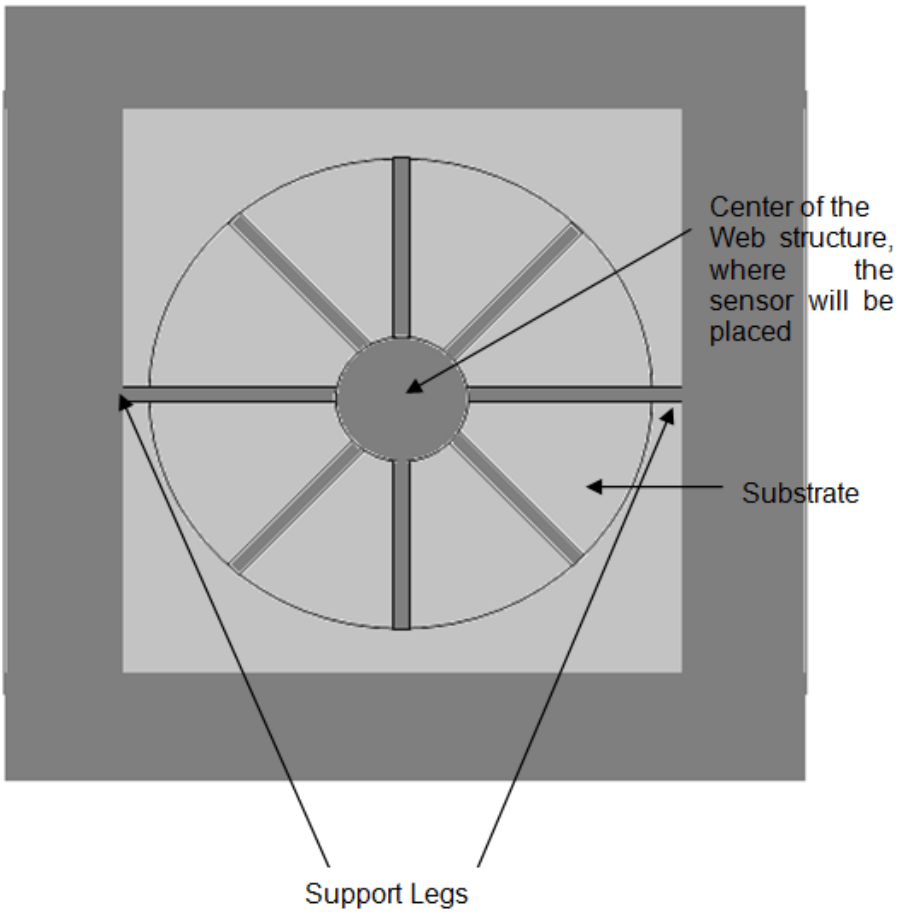

Figure 3.3 A simple web structure with two supporting legs connected to the substrate

The optical absorptivity of a micromesh absorber depends on the geometry as well as on the impedance of the absorbing metal film. A micromesh absorber will have a unique grid spacing g, and a line width a. R.Ulrich [37] has discussed a circuit model that was used to estimate the single pass absorption of the micromesh absorber as a function of frequency and the optimum resistance of the metal film. A freestanding lossy grid absorbs radiation with $\lambda \gg g$ with maximum efficiency when,

$$\rho \frac{g}{2at} = 189\ \Omega \tag{3.3}$$

where ρ the electrical resistivity of the metal film and t is its thickness. This equation implies that the edge to edge thermal conductance of the grid should be equal to 189Ω, in analogy with the optimal impedance for a freestanding solid film. One the web structure is

fabricated, a layer of a material which has high absorption is deposited on the structure to improve the absorption. A comparison was made based on a few journal papers to decide upon the start dimensions of the spiderweb structure, shown in the Table 3.1. First a square type device was designed. But the thermal conductivity between the sensor and the substrate was found to be high at certain legs. Legs are the beams which connect the sensor to the substrate and support the web. They also act as thermal connectors through which heat is transferred to the substrate. Since the square type design has a short coming of high thermal conductivity a circular type design was considered in this project. The dimension of the support leg has to be optimized to obtain proper support and low thermal conductivity.

Table 3.1 Dimensions of Spider web absorbers

Parameter	Thickness	Diameter of the absorber	Leg Dimensions
P.D.Mauskopf et al [36]	1μm	5.6mm	200μm long and 4μm wide
J.J.Bock et al [21]	1μm	2.5mm	1mm long and 5μm wide
F.B.Kiewiet et al [38]	1μm	1.4mm	0.55mm long and 5μm wide
J.M.Gildemeister et al [39]	1μm	3.5mm	1mm long and 7μm wide

Based on the comparison shown above it can be seen that the thickness of the web structure is assumed to be 1μm in all the designs. The width of each leg is found to be 5μm on the average, and the leg has a maximum length of 1mm. The study of the web structure dimensions has been carried out using FEM (Finite Element Method) software and the results are discussed in the next chapter.

3,4 Material selection and Fabrication

3.4.1.Substrate material

Silicon is used as the substrate material for almost all CMOS devices due to its excellent electrical and mechanical properties. Apart from these properties it has a very wide range of temperature of operation that extends upto 150°C (approx.). All these properties of silicon make it a suitable candidate, to act as the substrate material for MEMS devices. The electronic properties of silicon have been well used in the high volume CMOS manufacturing. Current micromachining and fabrication technologies utilize the mechanical properties of silicon to manufacture silicon substrates which hold high precision sensing elements.

3.4.2 Web structure

The web structure is made up of silicon nitride. Silicon nitride is one of the most attractive materials for MEMS devices due to its high mechanical strength and good electrical isolation. In the past silicon nitride has been used as one of the common absorbers for infrared detection. For example R.Lenggenhager et al, 1994, A.J.L.Adam et al, 2004 have used silicon nitride as the absorber layer to construct the infrared detector. P.J.French et al [40] have described the effects of deposition parameters of LPCVD silicon nitride. Silicon nitride is usually deposited by PECVD or LPCVD process. PECVD deposited silicon nitride is found to be contaminated by hydrogen atoms. The LPCVD process can be used to fabricate the web structure since it gives a better aspect ratio than PECVD. Usually for an LPCVD process, the important parameters are the process temperature, process pressure and flow rate. Since the spider web structure is constructed as a mesa structure, a sacrificial layer is first deposited and then silicon nitride is deposited. After the nitride is patterned the sacrificial layer is removed. PSG or polymide is usually used as the sacrificial layer. LPCVD silicon nitride is formed by reacting dichlorosilane ($SiCl_2H_2$) and ammonia (NH_3) within a temperature range of 700-800°C in a hot wall reactor (Wolf and Tauber, 1986). The chemical reaction is shown below,

$$3SiCl_2H_2\ (gas) + 4NH_3\ (gas) \longrightarrow Si_3N_4\ (solid) + 6HCl\ (gas) + 6H_2\ (gas)$$

The deposition rates of 10nm/min can be obtained at deposition temperatures of 700°C. The silicon nitride films obtained by LPCVD are found to be more stoichiometric than obtained by PECVD process. Dry etching can be performed on silicon nitride to obtain a better step coverage. The selectivity of silicon nitride to Si is 1:8 in the temperature range of 30-100°C. The properties of silicon nitride used for the simulation are shown in the table below,

Table 3.2 Properties of silicon nitride

PROPERTY	**VALUE**
Density (Wolf and Tauber, 1986)	2.5-2.8 g/cm^2
Thermal conductivity (www.memsnet.org)	30.1 W/m-K
Specific Heat (www.matweb.com)	0.7 kJ/kg-K
Dielectric constant (Wolf and Tauber, 1986)	6-9
Young's modulus (www.memsnet.org)	290 GPa
Poisson ratio (Senturia, “Microsystem Design”, p.196	0.27

3.4.3 Sensor material

The sensor material chosen for infrared radiation sensing is Ca-modified $PbTiO_3$ (Lead Calcium titanate). PCT is gaining a lot of attention in the recent years due to its high pyroelectric coefficient, and high detectivity. A. Tsuzuki [41] had demonstrated the fabrication and properties of PCT back in 1991. Lead titanate has very good piezoelectric, pyroelectric and ferroelectric properties. Lead titanate is said to have poor mechanical properties due to its large tetragonal ratio [42]. Calcium substituted lead titanate has gained a lot of attention because the addition of calcium gives better mechanical stability and better control over other properties of the material [43]. PCT can be deposited by RF magnetron sputtering or by sol-gel method. Usually sol-gel method results in yielding very good properties from the material than by sputtering. Sol-gel

process is a versatile method used to deposit ferroelectric materials. Sol-Gel technique involves in the transformation of a system from a liquid sol into a solid gel phase. The precursor materials used for the deposition are usually inorganic metal salts or metal organic compounds. The sol-gel process used to deposit PCT is shown in Figure 3.4,

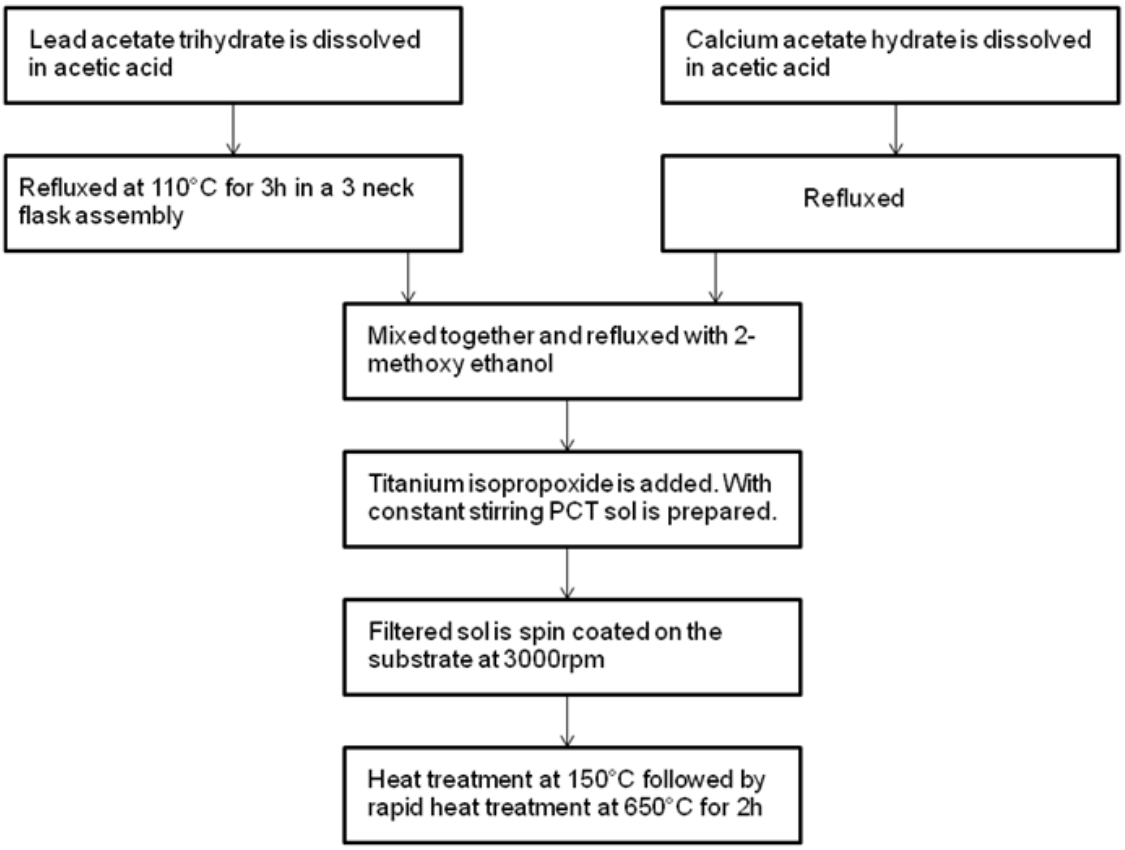

Figure 3.4 Sol-gel preparation of PCT thin film [42]

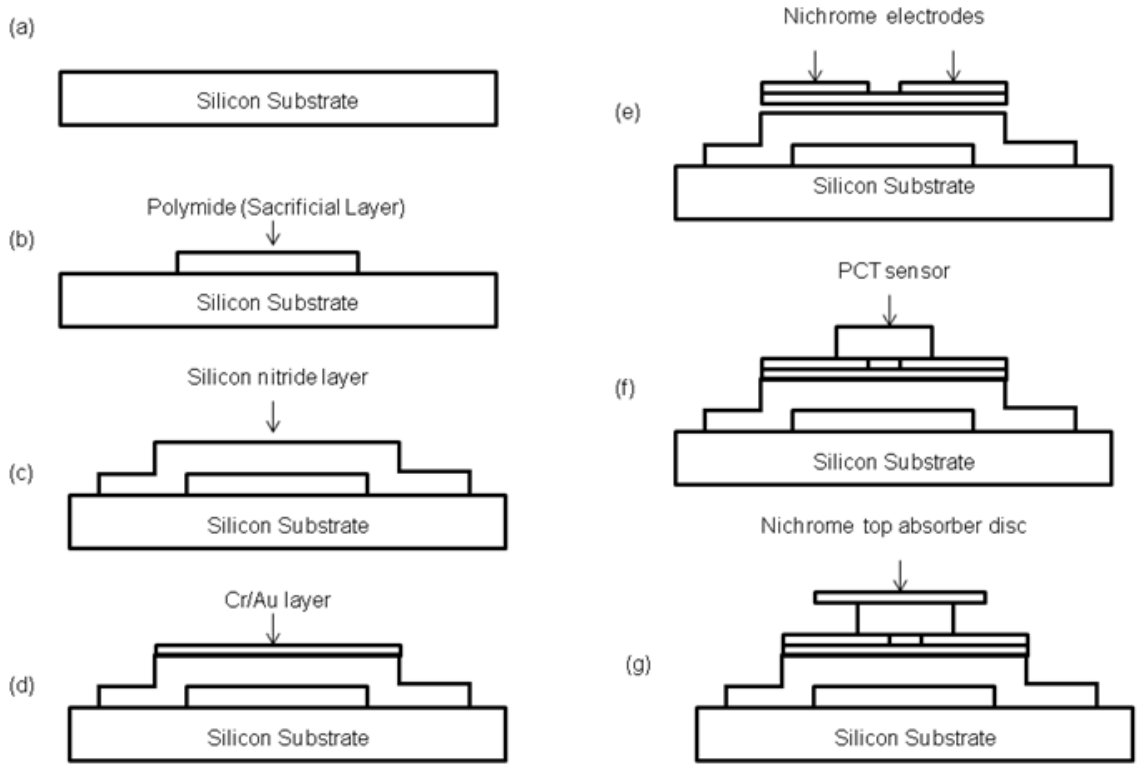

Figure 3.5 Cross-section of the proposed pyroelectric infrared sensor

First the silicon substrate is cleaned to remove any contaminations. Usually RCA clean is done to ensure that the wafer is clean. The processing starts as soon as the cleaning finishes as an oxide layer is developed if the wafer is stored in a container. Then the sacrificial polymide layer is deposited. This layer is used to form the elevated mesa structure (b). It is etched after the deposition of silicon nitride. Silicon nitride layer is deposited by LPCVD process. The web structure is dry etched on the silicon nitride layer. A Cr/Au layer is deposited (c) on the center mesh to improve absorption. The web structure is not seen in the above diagram since it shows the cross-section of the device. Then the nichrome electrodes are deposited on the web structure. Since electrodes are thin and long they have to be carefully deposited. They have to be aligned accurately with one of the supporting legs of the web structure. Nichrome is usually deposited using RF sputtering. The PCT sensor is derived by sol-gel method. It is first deposited on a glass substrate (f). The sensor is then bonded to the center of the web structure. The top

nichrome disc is deposited also by RF sputtering (g). Care must be taken to make sure that the disc does not get deformed during the fabrication process.

3.5 Conclusion

Photon detectors are fundamentally limited by generation-recombination noise arising from photon exchange with a radiating background. On the other hand thermal detectors are fundamentally limited by temperature fluctuation noise arising from the radiant power exchange with a radiation background. This effect of temperature fluctuation can be compensated by comparing the output from a detector which is not exposed to the input infrared radiation. Good absorber designs also help in reducing this effect. Two absorbers for the proposed pyroelectric sensor have been discussed, and presented with appropriate calculations. The material selection for each part of the pyroelectric detector has been studied. The fabrication principles and the probable fabrication methodologies have been discussed. The fabrication methods can vary based on the thickness of each part of the sensor. The thickness and other dimensions of the pyroelectric detector are studied in the next chapter.

CHAPTER 4

SIMULATION OF THE THERMAL TRANSIENTS

4.1 Overview

The design and analysis of the pyroelectric detector is done using FEM method. Coventorware is used to design the fabrication steps, create a layout mask design for each layer and generate a 3-D model. The following design steps are used to create the 3-D model of the device structure in Coventorware,

a) Material definition

b) List of Process steps

c) Layout design (Mask design of each layer defined in the process steps)

d) Generate a 3-D model using DESIGNER (and define names for volumes and patches)

e) Mesh sensitivity analysis

f) Thermal Analysis

The thermal analysis mentioned here is performed to find out the thermal conductivity of the sensor to the substrate. This value must be as low as possible so that the sensor can absorb maximum temperature change and generate the corresponding charges. If there is a very good thermal path between the sensor and the heat sink (substrate), then the heat flows into the sink thereby reducing the sensitivity of the sensor. FEM method is a well known method used to solve partial differential equations and arrive at an approximate result of an engineering problem. It is used extensively to solve thermal heat transfer, strain-stress analysis and even in automobile engineering to predict the damage caused by an accident. The basic principle behind finite element analysis is that the solver divides the given problem or block of material (designed in 3-D into finite number of small parts and applies the differential equations to each part and sums the result of every individual part. The process of dividing the 3-D model

into individual parts is called meshing. Meshing is very important aspect of FEM analysis as, meshing decides the run time, the processing power required to run the solver, the accuracy of the final result, and other important parameters of the result. Mesh sensitivity analysis has to be performed in any 3-D model to fine tune the accuracy of the obtained result. It is the process of increasing the number of elements until a constant output is obtained. The mesh sensitivity analysis performed on the current model is shown below:

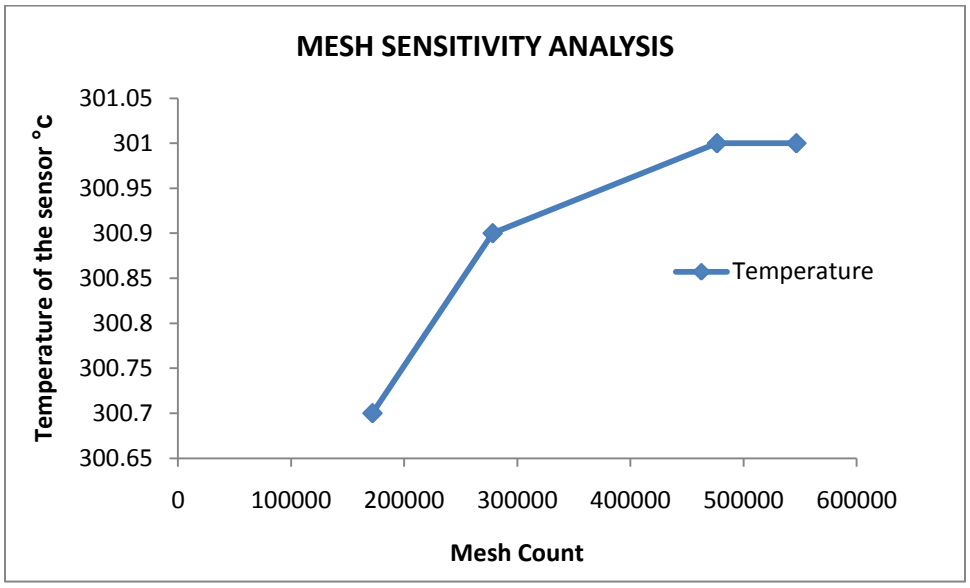

Figure 4.1 Mesh sensitivity analysis

Coventorware Memmech is the tool in Coventorware which is used to perform mechanical and thermal analysis on 3-D microstructures. The materials which are going to be used in the fabrication of the MEMS device are first updated in the material properties database. All the properties mentioned in the previous chapter is entered as shown in the figure 4.2,

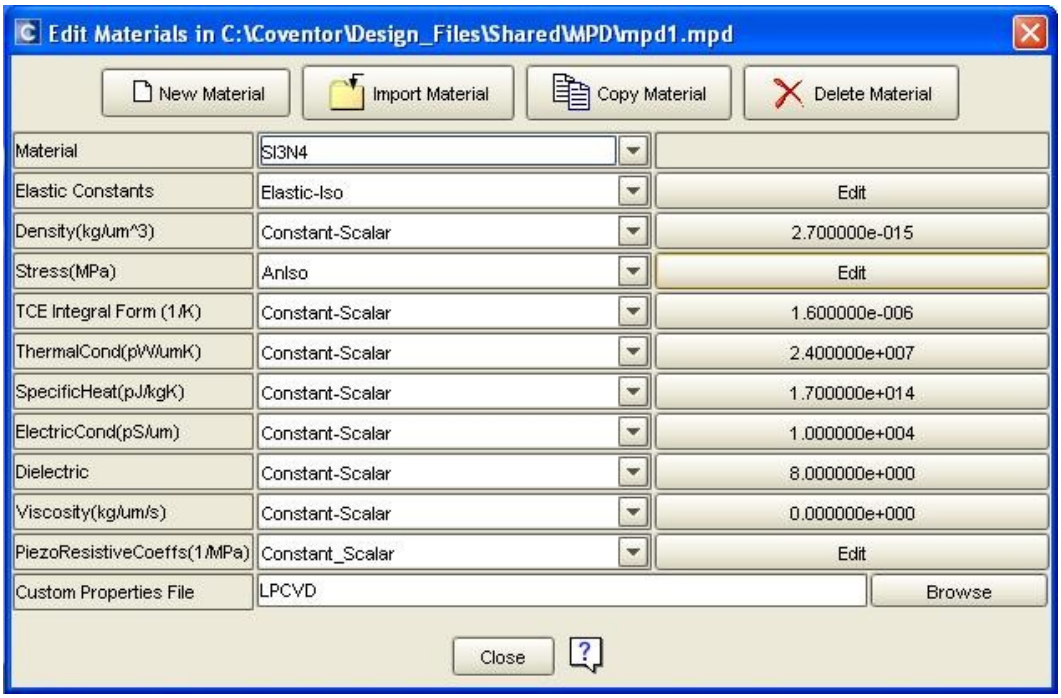

Figure 4.2 Material Definition of Silicon Nitride in Coventorware

The layout designs are then drawn based on the dimensions calculated on the device. The layout is a combination of masks of each process step involved in the fabrication process. The process steps are defined in the process editor tool. Various inbuilt process like lift-off, wet etching, dry etching, planar fill etc, in Coventorware makes it really easy to define the process steps involved in the fabrication. The final 3-D model of the device structure is shown below:

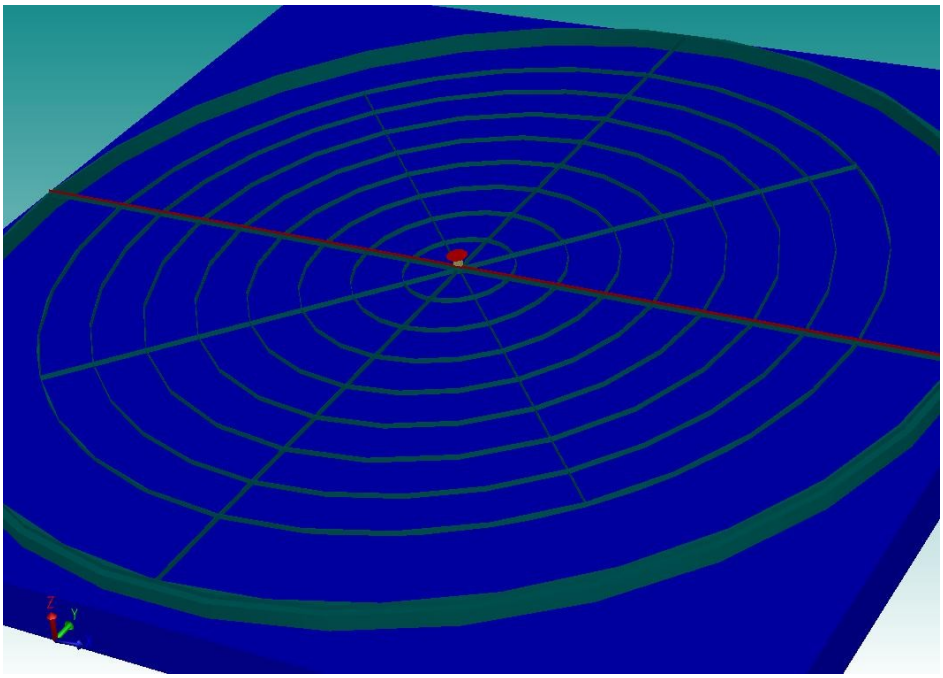

Figure 4.3 The 3-D model of the proposed Pyroelectric Detector

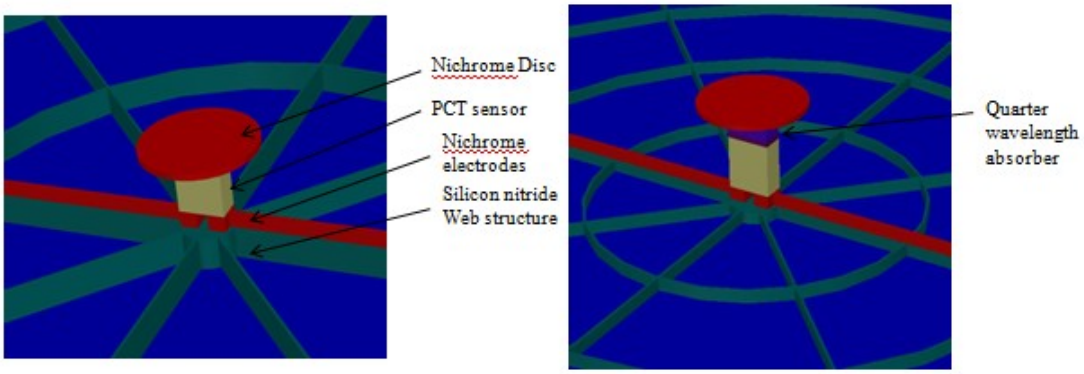

Figure 4.4 Spider web structure view with the sensor and the quarter wavelength absorber

The Spiderweb structure is clearly seen in the 3-D model. The number of slots in the spiderweb structure has been varied and simulated but no significant change in the thermal conductivity has been detected. The Dimensions of the infrared sensor is shown in the table below:

Table 4.1 Dimensions of the proposed device

Dimensions of the top disc	Radius of the disc =10μm, thickness =0.2μm
Dimensions of the web structure	Radius of the web structure = 100μm, the length of the supporting leg (end to end) =225μm, thickness = 0.3
Dimensions of the sensor	8μmx4μm (rectangular), thickness of 2μm
Dimensions of the electrode	Top head = 3μmx4μm, length =235μm, thickness = 0.1 or 0.5
Dimensions of the device as a whole	270μmx270μm

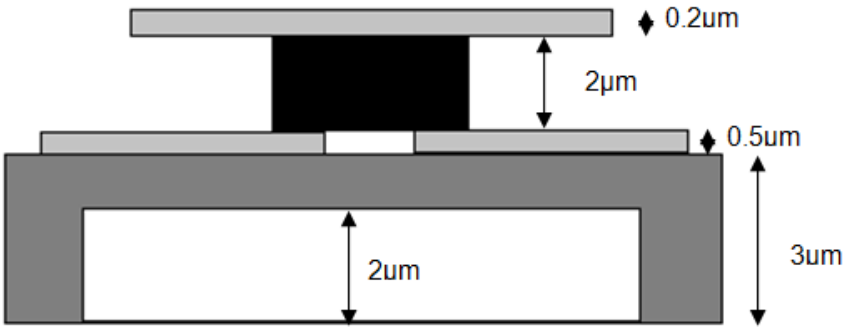

Figure 4.5 Dimensions of the proposed pyroelectric detector

4.2 Study of variation of the thickness of the web-structure

As mentioned earlier the thickness of the web structure is usually 1μm. But the main aim of this research is to reduce the size of the infrared sensing device thereby reducing the thermal conductivity between the sensor and the substrate. This effect improves the sensitivity of the sensor material. The thickness of the web-structure was considered from 0.1μm to 1μm. This gives us an idea about the possible thickness of the silicon nitride layer to construct the web structure, which can be mechanically strong as well as have less thermal conductivity. Along with the thickness analysis, the lengths of the supporting legs are also varied. The length of the supporting legs starts from as low as 20μm. Thermal transient analysis has been performed on the device. The boundary conditions for the analysis are set. To start with all the

volumes are maintained at 300 K and a heat flux of 50 pw/μm^2 is applied on the top disc (patch). The Top substrate patch is kept at a constant room temperature of 300 K. The thermal link is an important parameter that has to be defined in Coventorware to establish thermal connection between the layers of the device.

Table 4.2 Thermal conductance in comparison with the radius of the web

Radius of web (μm)	**Thermal conductance (W/K)**
20	1.396×10^{-7}
25	1.067×10^{-7}
30	8.078×10^{-8}
35	7.125×10^{-8}
40	6.129×10^{-8}
45	5.5319×10^{-8}
55	4.429×10^{-8}
60	2.80×10^{-8}
65	1.749×10^{-8}
70	1.65×10^{-8}
80	1.47×10^{-8}
90	1.570×10^{-8}
95	1.049×10^{-8}
100	9.514×10^{-9}

Thus the radius of the web structure was found to be 100μm if a thermal conductivity in the order of 10^{-9} W/K had to be obtained. Now the device is further analyzed for longer web structures for varying thickness.

Table 4.3 Thickness of the web structure = 0.1μm

Radius of the web (μm)	**Thermal Conductivity (W/k)**
100	$1.07x10^{-7}$
300	$4.259x10^{-8}$
500	$2.66x10^{-8}$
700	$1.96x10^{-8}$
900	$1.55x10^{-8}$

Table 4.4 Thickness of the web = 0.3μm

Radius of the web (μm)	**Thermal Conductivity (W/k)**
100	$2.27x10^{-7}$
300	$9.17x10^{-8}$
500	$5.81x10^{-8}$
700	$4.28x10^{-8}$
900	$3.378x10^{-8}$

Table 4.5 Thickness of the web structure = 0.5μm

Radius of the web (μm)	Thermal Conductivity (W/k)
100	$1.57x10^{-7}$
300	$1.396x10^{-7}$
500	$8.97x10^{-8}$
700	$6.61x10^{-8}$
900	$5.235x10^{-8}$

Table 4.6 Thickness of the web structure =1μm

Radius of the web (μm)	Thermal Conductivity (W/k)
100	$1.05x10^{-7}$
300	$2.61x10^{-7}$
500	$1.67x10^{-7}$
700	$1.244x10^{-7}$
900	$9.66x10^{-8}$

4.3Thermal Conductance G_{th} calculation

Radius of the Disc = 10μm

Area of the disc = $\pi r^2 = \pi * 10^2 = 100\pi\ \mu m^2$

Heat flux applied on top of the disc = 50 pw/μm^2

⇨ $100\pi * 50 * 10^{-12} = 1.570 * 10^{-8}$ W/μm^2

G_{th} (301.651-300) = $1.570 * 10^{-8}$

$G_{th} = \frac{1.570 * 10^{-8}}{1.651} = 9.51 * 10^{-9}$ W/K

Thus it is found that the thermal conductivity from the sensor to the substrate as low as $9.51*10^{-9}$ W/K. This value is found to be really low thereby increasing the sensitivity of the

device by holding the heat within the sensor and not transferring it to the heat sink. The study of the various thickness of the web structure has been performed keeping the thickness of the electrode as 0.5µm. But fabrication of nichrome can be performed and based on the mechanical stability of the device the thickness can be reduced up to 0.1µm. With the thickness of the electrode as low as 0.1µm thermal conductivities in the order of 10^{-10} to 10^{-12} are achievable with the proposed device. The transient analysis performed on the device is graphically shown below; the red line indicates the sensor temperature, and the green line shows the web structure temperature. The graph clearly indicates the sensitivity of the sensor for the corresponding input heat flux.

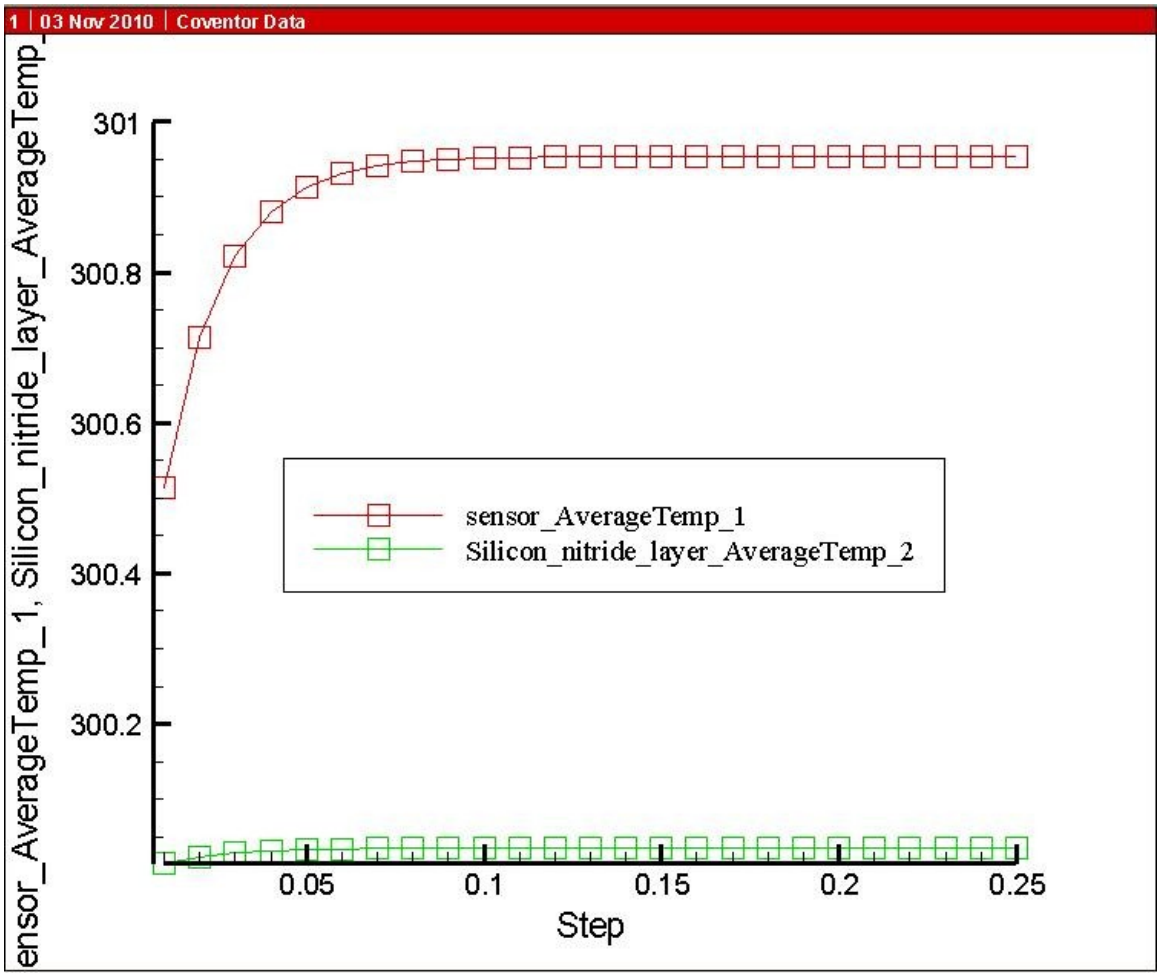

Figure 4.6 Sensor temperatures vs. time (Transient analysis)

Thermal Capacitance:

We know that,

$$\tau_{th} = \frac{C_{th}}{G_{th}}$$

G_{th}= 9.51x10^{-9} W/K, τ_{th} = 0.02 sec (from the graph: time taken to attain 63.2% of the final value)

C_{th} = 1.902 x10^{-10} J/K

4.4 Characteristics of the device

4.4.1 Voltage responsivity vs. Frequency

The selection of the time constants τ_{th}, τ_{ele} in the voltage responsivity equation (given below from the previous chapter), and thus the control of the frequency response, depends on the application where the sensor is to be used. The voltage responsivity of an infrared sensor is given as,

$$R_v(\omega) = \frac{p\eta\omega A R_p}{G\sqrt{1+\omega^2\tau_{th}^2}\sqrt{1+\omega^2\tau_{el}^2}}$$

If a low frequency, high sensitivity operation is required the device will have be mounted on a mesa structure there by providing necessary isolation from the substrate, improving the sensitivity of the device. The device is freely suspended as possible. Usually 8μm to 15μm region of the infrared spectrum falls under this category (human detection application is in this region of the infrared spectrum). The following table indicated the voltage response with respect to the chopper frequency.

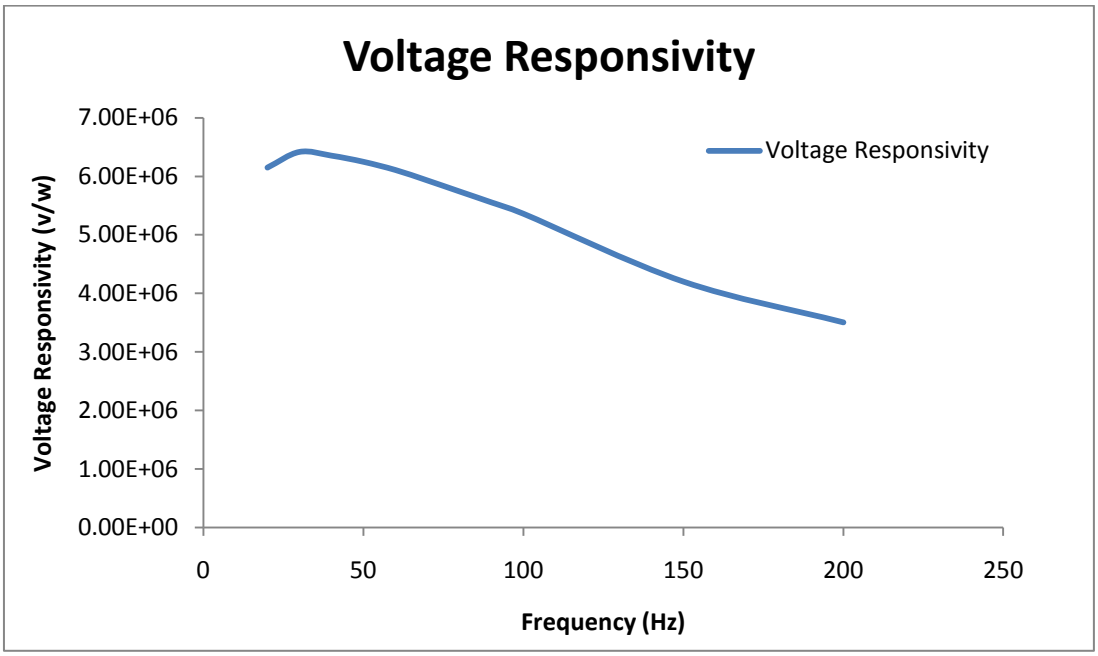

Figure 4.7 Voltage responsivity (vs.) Frequency

Using the time constants $\tau_{th}\ and \tau_{ele}$ the lower and upper cut off frequencies are calculated using the formula $f = \frac{1}{2\pi(\tau_{th},\tau_{ele})}$. The frequency is varied from 20 to 100 Hz with step interval of 10Hz are calculated and shown in the graph. It is seen that the voltage responsivity is high at lower frequencies and decreases as the chopper frequency increases. A maximum voltage responsivity of 6.94E+07 is obtained at 10Hz. The absorptivity η is assumed to be equal to 1. $\omega = 2\pi f$ is the angular frequency and was calculated for each frequency. The thermal and electrical time constants $\tau_{th}\ and\ \tau_{ele}$ are found to be 0.02 sec and 0.00122 sec. R_p is assume to be 100 GΩ. The thermal conductivity G_{th} = 9.51x10^{-9} W/K (from the simulation results). The area of the detector A is calculated as 0.00000028 cm^2 and the pyroelectric coefficient used for the calculations is 46x10^{-9} C/cm^{2}K.

4.4.2 Detectivity Vs frequency

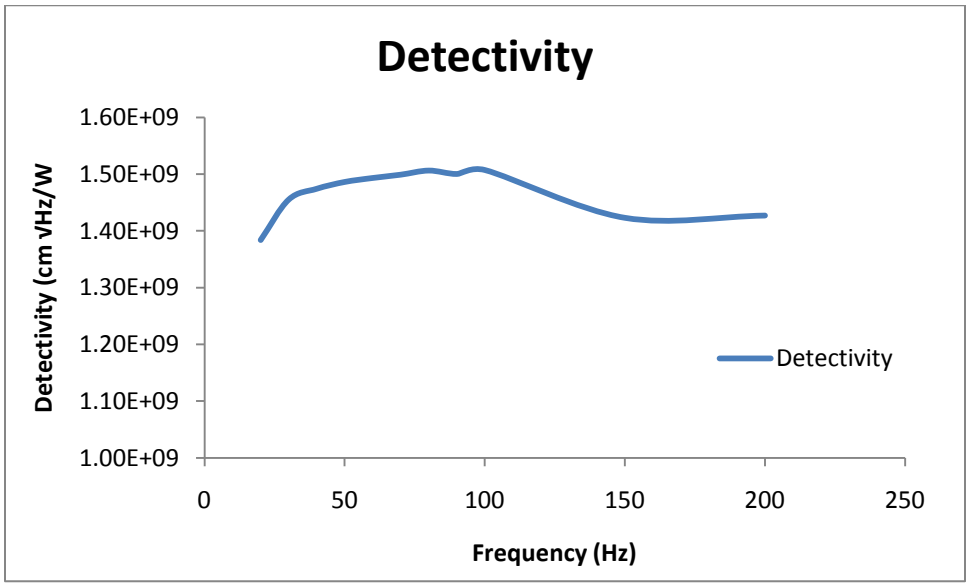

Figure 4.8 Detectivity (vs.) Frequency

The detectivity of the detector is obtained in the order of 10^9 cm √Hz/W. We see that the detectivity is almost constant in the frequency range 10-100Hz. Such high detectivity shows that the noise equivalent power of the device is really low. The noise parameters of the device is plotted in the figures 4.9, 4.10 and 4.11.

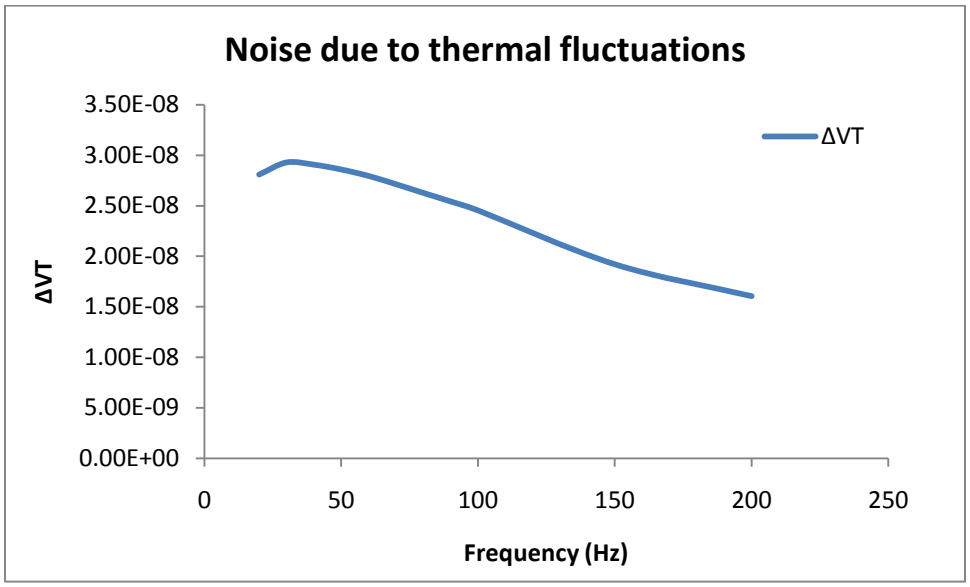

Figure 4.9 Noise due to thermal conductance

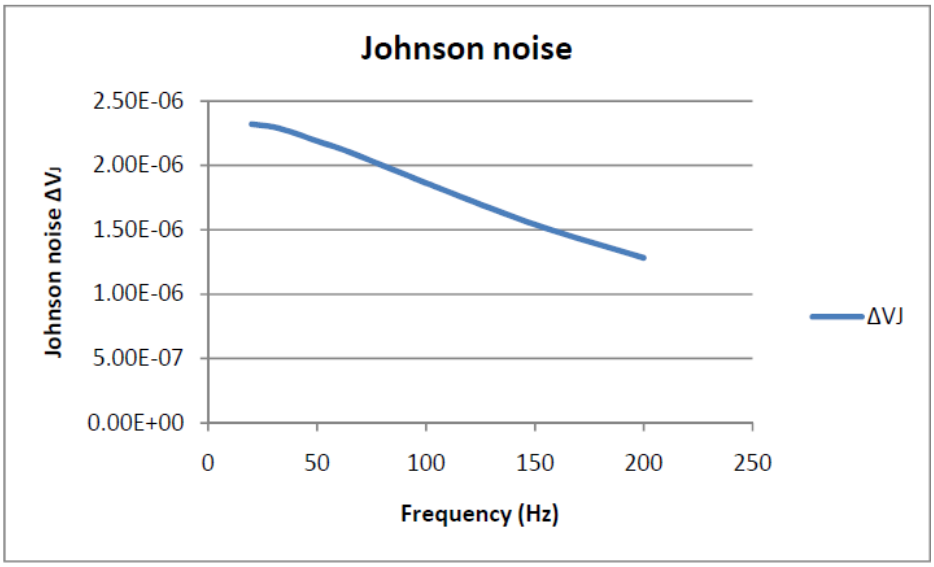

Figure 4.10 Johnson noise

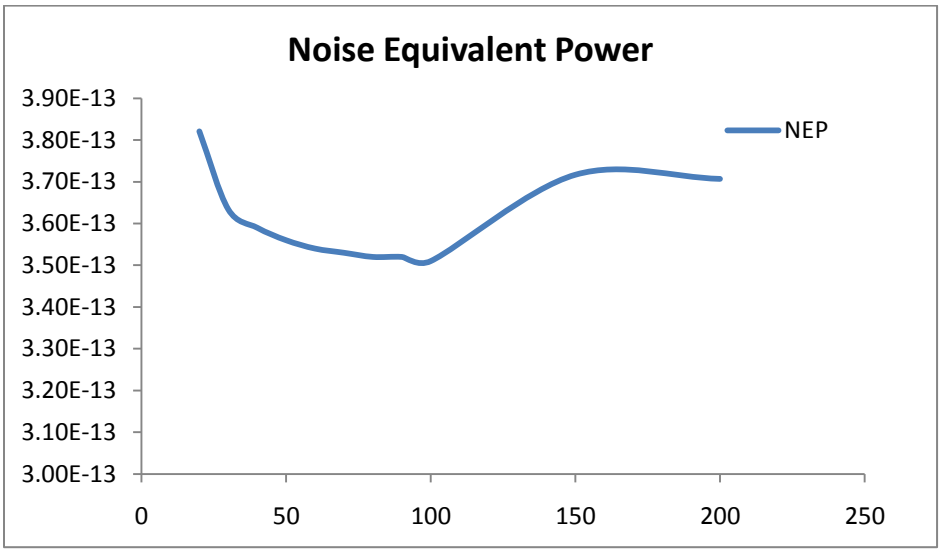

Figure 4.11 Noise equivalent power

4.5 Antenna Analysis

To find out the efficiency of the reception of the device an Antenna analysis was performed on the device. The structure was designed as a Microstrip Patch Antenna and antenna analysis was done on the structure. ADS-Genesys is used to perform an antenna analysis for a wide variety of antenna's. There are two main tools in ADS-Genesys that runs electromagnetic simulations they are

1) EMPOWER: It is used to perform the S-parameter (Scattering parameter analysis)

2) MOMENTUM: It does 3-D analysis and displays a 3-D view of the sensitivity of the antenna

4.6 Microstrip Patch Antenna overview

A microstrip antenna consists of conducting patch on a ground plane separated by dielectric substrate. Various mathematical models were developed for this antenna and its applications were extended to many other fields. Low dielectric constant substrates are generally preferred for maximum radiation. The conducting patch can take any shape but rectangular and circular configurations are the most commonly used configuration. A microstrip antenna is characterized by its Length, Width, Input impedance, and Gain and radiation patterns. The length of the antenna is nearly half wavelength in the dielectric; it is a very critical

parameter, which governs the resonant frequency of the antenna. The mechanisms of transmission and radiation in a microstrip can be understood by considering a point current source (Hertz dipole) located on top of the grounded dielectric substrate. This source radiates electromagnetic waves. Depending on the direction toward which waves are transmitted, they fall within three distinct categories, each of which exhibits different behaviors.

1) Surface waves

2) Leaky waves

3) Guided waves

There are many factors like polarization, the type of feed which affects the efficiency of the antenna to receive and radiate electromagnetic energy. As the goal is not to design a microstrip antenna we are interested in the resonant frequency, radiation patterns, and the directivity of the structure.

4.7 Feed Techniques

Microstrip patch antenna's can be fed by a variety of methods. The methods by which the energy is input to the system can be divided into two, i) Contacting type ii) Non-Contacting type. In the contacting method, the RF power is fed directly to the radiating patch using a connecting element such as a microstrip line. In the non-contacting scheme, electromagnetic field coupling is done to transfer power between the microstrip line and the radiating patch. The four most popular feed techniques used are the microstrip line, coaxial probe (both contacting schemes), aperture coupling and proximity coupling (both non-contacting schemes).

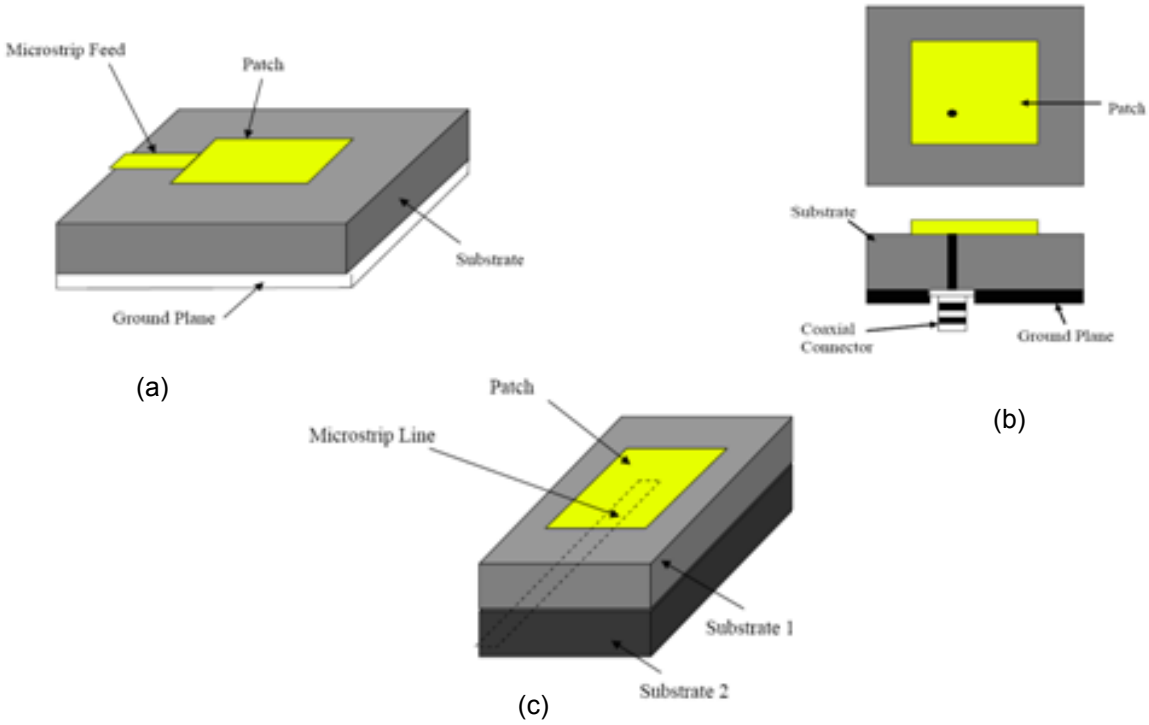

Figure 4.12 a) Microstrip line feed, b) Coaxial line feed c) Proximity coupled feed

This type of feed technique is called as the electromagnetic coupling scheme. As shown in Figure 5.4, two dielectric substrates are used such that the feed line is between the two substrates and the radiating patch is on top of the upper substrate. This type of feed is comparable to our design. The layout is designed next. The layout design is shown below:

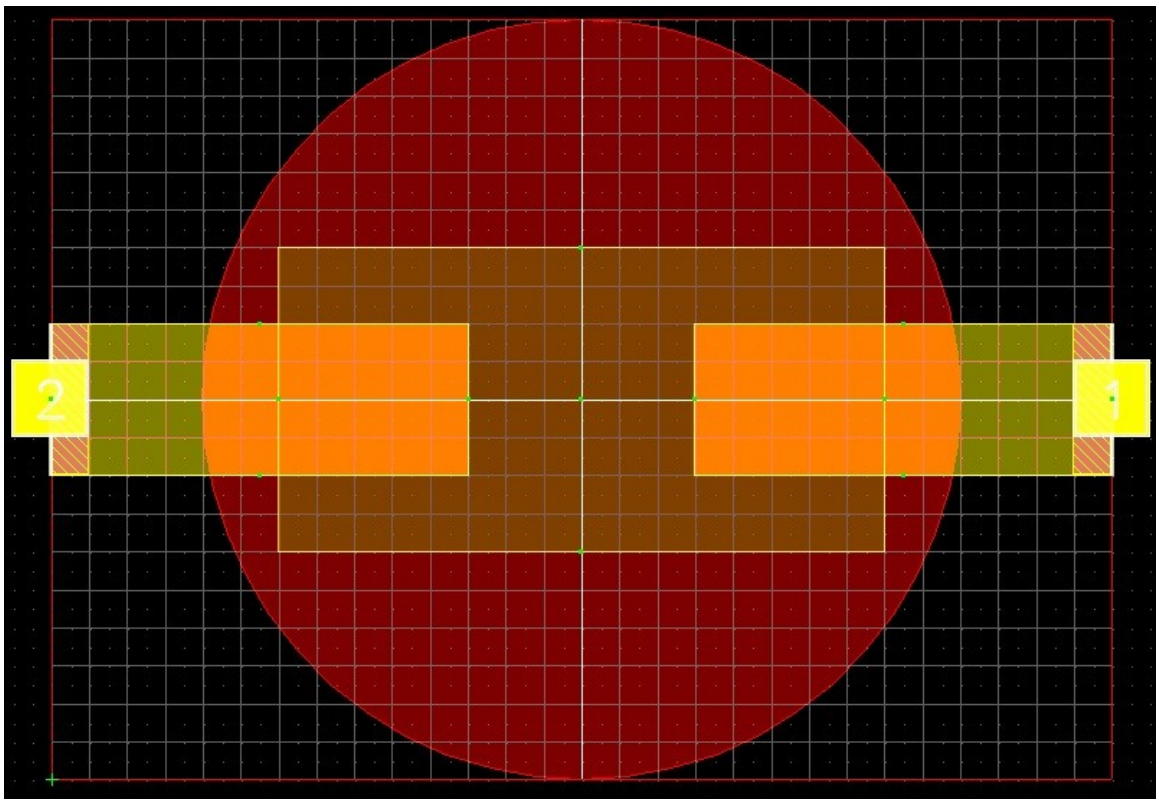

Figure 4. 13 Antenna layout design

Two feed lines have been designed with two electromagnetic ports 1 and 2. The rectangular box seen in the center is the substrate. All the dimensions are the same as the Coventorware design. The top disc has material properties of nichrome and the dimensions of the nichrome disc. The ADS Momentum simulations were simulated. The s-parameter graph is shown below. The resonant frequency is found in the terahertz region as calculated (Infrared waves have their wavelength in μm range, so the resonant frequency must be in the terahertz range) .The results are shown in the figure 4.14,

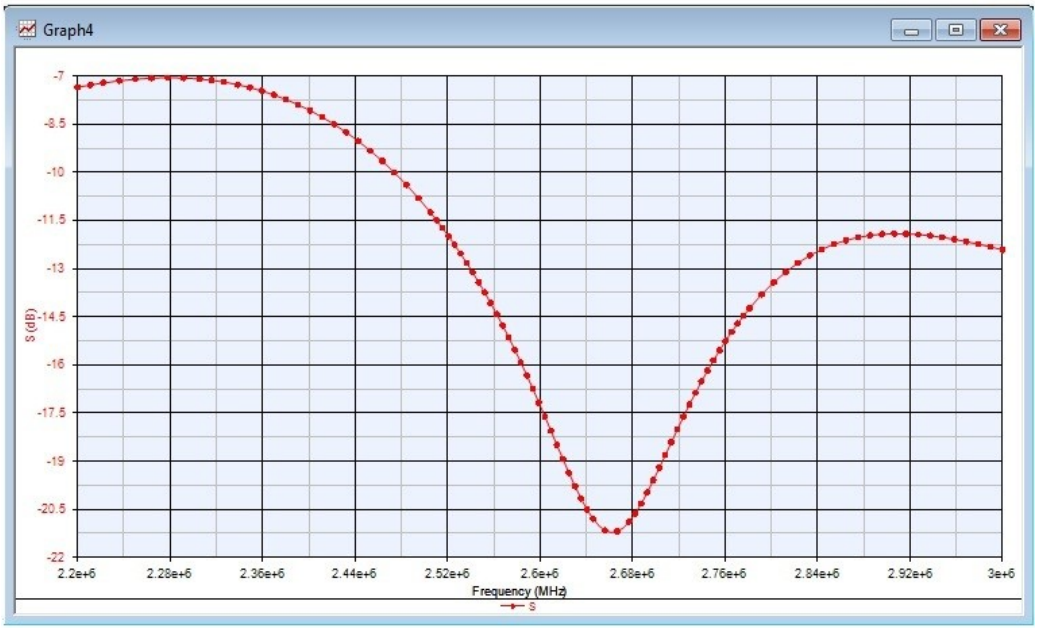

Figure 4.14 S-parameter graph

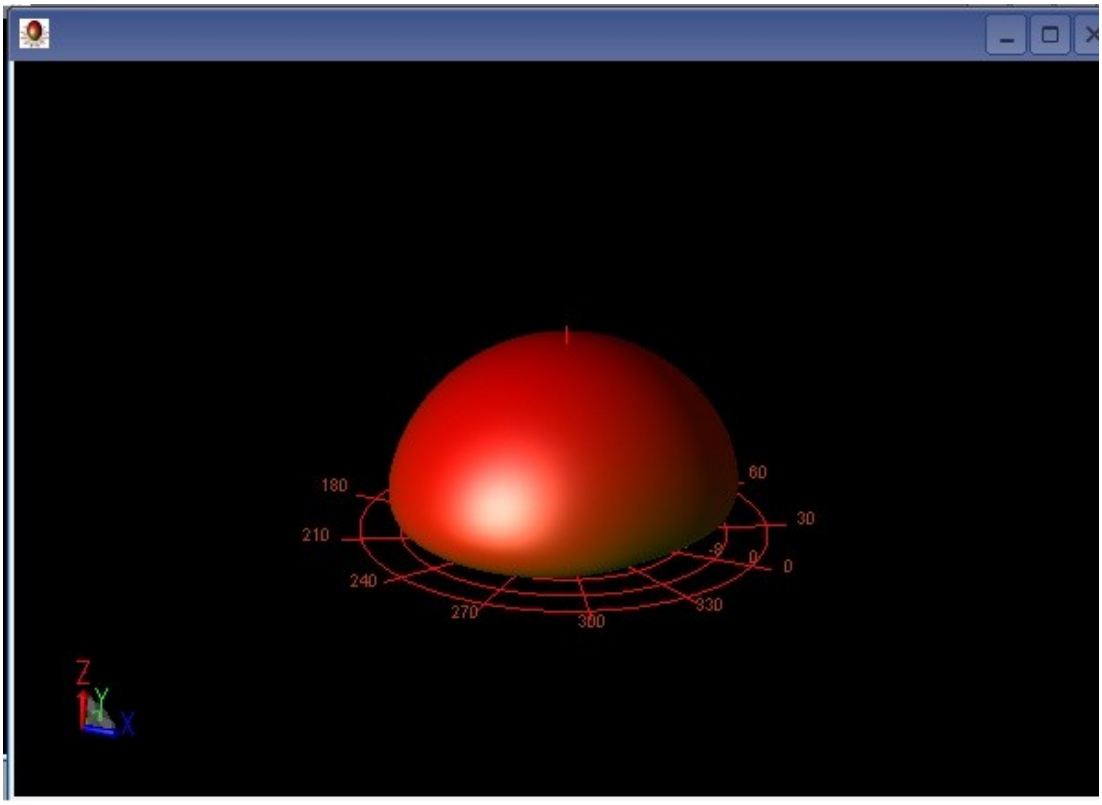

Figure 4.15 Radiation patterns

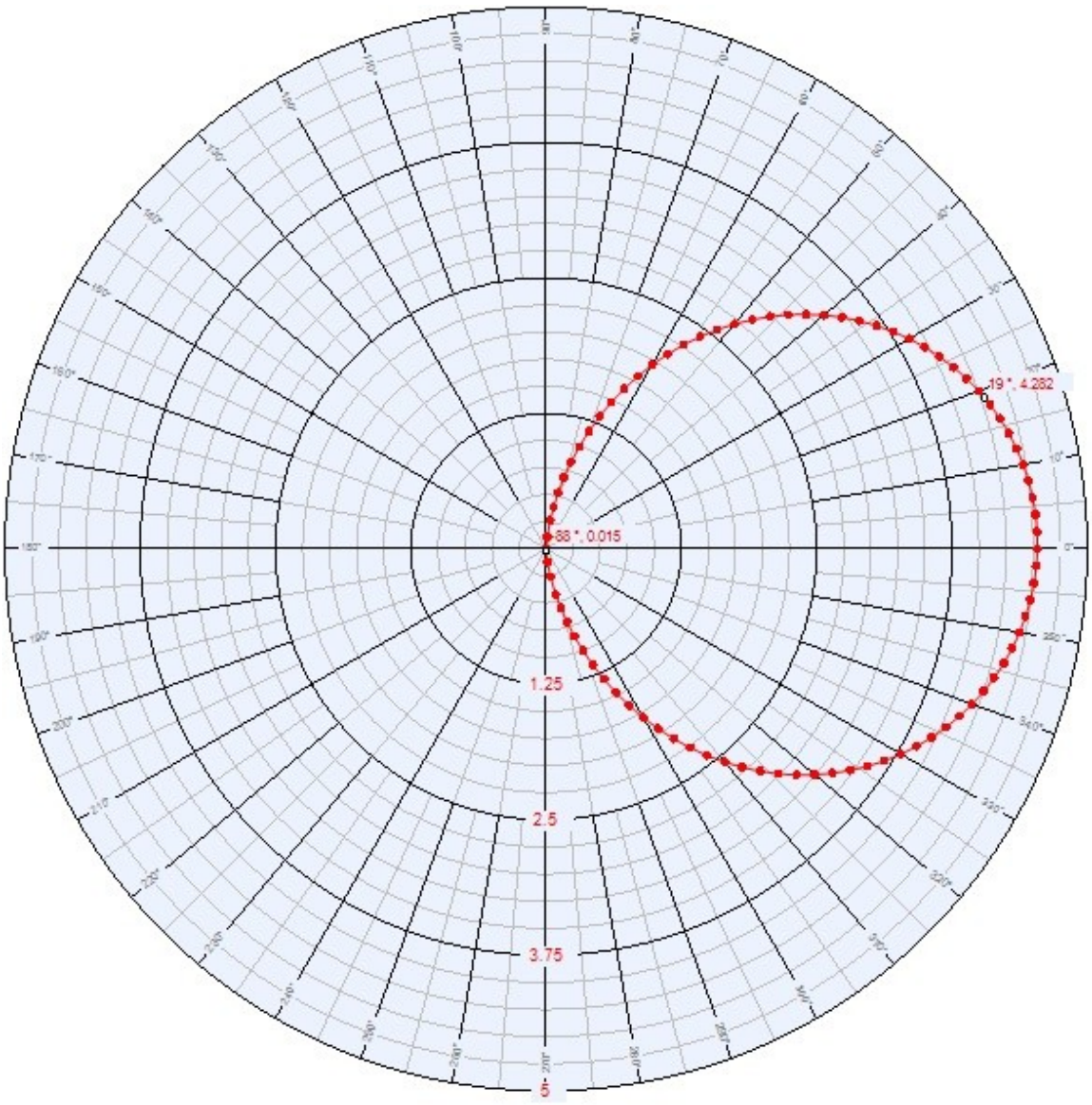

Figure 4.16 Directivity graph

Since a microstrip patch antenna radiates normal to its patch surface, the elevation pattern for φ = 0 and φ = 90 degrees would be important. The center frequency of this antenna was found from the s-parameter graph as 2.6 THz. The maximum gain is obtained in the broadside direction. The back lobe is not obtained because ADS momentum considers an infinite substrate. The 3D plots for the antenna directivity are shown above. A maximum directivity of 6.04773 dBi is obtained from the plot.

4.8 Conclusion

Thus the device model was simulated using Coventorware. First the material definition was done. Various constants such as young's modulus, thermal conductivity, resistivity of the materials used in this model (Nichrome, PCT, and Silicon Nitride) were declared at the beginning in the material definition window. Then a layout mask was created based on the dimensions of the device. Before the layout mask creation the process steps are defined. The process fabrication steps are specified. Then a 3-D model is created using the Designer in Coventorware. The model is meshed. The mesh values are decided after proper mesh sensitivity analysis is done. Different patches where the heat flux needs to be applied and thermal linkages have to be created are marked. Then using Analyzer tool the meshed model is solved. The simulation time, thermal linkages, room temperature, and the amount of heat flux are specified in the solver setup and then the simulation is run. The simulation time can be adjusted based on the meshing setup and the simulation time. Thus the transient analysis was performed. For the antenna analysis, again material definition was done, and a layout of the top of the device is created. The 3-D model can be viewed using the 3-D model viewer. Then a momentum simulation is run for a wide range of frequencies. The center frequency is found from the s-parameter graph. Then the directivity of the antenna is found from the far field simulations.

CHAPTER 5

CONCLUSIONS AND FUTURE WORK

The design and fabrication of pyroelectric infrared sensors have been discussed based on simulation results. The amount of increase in sensitivity that can be obtained using PCT (72/28) as the sensor material and a mesh of lossy wires as the absorbing structure (spider web in this case) was discussed. The voltage responsivity of the device was calculated as $6x10^{6}$ V/W. The Detectivity of the device was calculated as and $1.52x10^{9}$ cm $\sqrt{}$Hz/watt. The quarter wavelength absorber if fabricated could result in a very high sensitivity detector. According to the theoretical calculations, it yields more than 96% of the heat falling on the surface. The thermal conductance between the sensor and the substrate (heat sink) is obtained as low as G_{th}= $9.51x10^{-9}$ W/K compared to the radiative thermal conductance of $3.69x10^{-7}$ W/K. Such low thermal conductivity yields a high sensitivity detector. The spider web structure along with a thin layer of metal deposition could increase the absorptivity of the device to a significant level. The mask designs of each individual layers have been clearly laid out. The mesh sensitivity analysis has been performed on the structure which implies that the value of thermal conductivity got by the thermal transient analysis through Coventorware is an accurate value. The device can now be fabricated using the mask designs available. In the future the quarter wavelength absorber can be implemented in the antenna analysis in an electromagnetic solver and the efficiency of the top structure of the device can be found. The absorption of the device and hence the sensitivity of the PCT sensor will be maximum if the quarter wavelength absorber works along with the spider web absorber. The fabrication of the quarter wavelength structure and the spider web structure can be done separately and the results can be compared to get a better idea about the structure under practical conditions. The major advantage of this type of thermal

device is that it does not need external cooling, which improves the efficiency of the detector by a great factor.

REFERENCES

1) Tohru Iuchi and Aiji Jono, "***New radiation thermometer for near room temperature***", Measurement Volume 16, Issue 4, 1995, pp 257-263

2) M.F. Ugarte, A.J. de Castro, S. Briz, J.M. Aranda, F. Lo´pez, **"*Optimized geometry in infrared arrays for remote sensing of forest fires***", Infrared Physics & Technology, Volume 41, 2000, pp 35–39

3) Franco Baldi, Ermanno Cozzani, Marco Filippelli, "***Gas chromatography/Fourier transform infrared spectroscopy for determining traces of methane from biodegradation of methylmercury***", Environmental science and technology, Volume 22 issue7, pp 836–839, 1988

4) Kateb B, Yamamoto V, Yu C, Grundfest W, Gruen JP, "***Infrared thermal imaging: a review of the literature and case report***", Neuroimage volume 47 Suppl 2, 2009, pp 154-62

5) A. Rogalski, "***Competitive technologies of third generation infrared photon detectors***", Opto-electronics review volume 14 issue1, 2006, pp 87–101

6) Bajaj, J., "***HgCdTe infrared detectors and focal plane arrays***", Optoelectronic and Microelectronic Materials Devices, 1998, pp 23 - 31

7) A Rogalski, "***HgCdTe Infrared detector material: History, status and outlook***", Reports on Progress in Physics, Volume 68, Number 10 2005, pp 2267-2336

8) Antoni Rogalski**, "*Infrared detectors: status and trends***", Progress in Quantum Electronics Volume number 27, Issue numbers 2-3, Year 2003, pp 59-210.

9) Antoni Rogalski, "***Infrared thermal detectors versus photon detectors: I. Pixel performance***", Material science and material properties for infrared optoelectronics, proceedings volume 3182, 1997 pp-14-25

10) J. Piotrowski and A. Rogalski, "***Uncooled long wavelength infrared photon detectors***", Quantum Sensing and Nanophotonic Devices, Proc. of SPIE Volume 5359, pp115-131

11) Simon M.Sze, "***Semiconductor Sensors***", Wiley-Interscience, October 1994, ISBN 978-0471546092

12) R J Dickinson, "***Thermal conduction errors of manganin-constantan thermocouple arrays***", Physics in Medicine and Biology Volume 30, Number 5 1985, pp 445-453

13) Lahiji, G.R. Wise, K.D., "***A batch-fabricated silicon thermopile infrared detector***", Electron Devices, IEEE Transactions on Electron devices Volume 29 Issue1 982 pp 14 – 22

14**)** A.W. Van Herwaarden and P.M. Sarro**, "*Thermal sensors based on the seebeck effect***", Sensors and Actuators Volume 10, Issues 3-4, 1986, pp 321-346

15) L. P. Boivin and T. C. Smith, "***Electrically calibrated radiometer using a thin film thermopile***", Applied Optics, Volume 17, Issue 19, 1978, pp 3067-3075

16) David R. Lide, "***Handbook of Chemistry and Physics***" 81st Edition, CRC Press, 2000 ISBN-13: 978-0849304811

17) Nguyen Chi-Anh, Hyun-Joon Shin, KunTae Kim, Yong-Hee Han and Sung Moon, **"*Characterization of uncooled bolometer with vanadium tungsten oxide infrared active layer***", Sensors and Actuators Volumes 123-124, issue 23, 2005, pp 87-91

18) E. Monticone*, L. Boarino, G. Lérondel, R. Steni, G. Amato and V. Lacquaniti, **"*Properties of metal bolometers fabricated on porous silicon***", Applied Surface Science, Volume 142, Issues 1-4, 1999, pp 267-271

19) M. Gonzalez and E.R. Hodgson, **"*Electrical and mechanical behavior of improved platinum on ceramic bolometers***", Fusion Engineering and Design Volume 82, Issues 5-14, pp 1277-1281

20) Jian-Gong Cheng, Xiang-Jian Meng, Jun Tang, Shao-Ling Guo, and Jun-Hao Chu, "***Pyroelectric Ba0.8Sr0.2TiO3 thin films derived from a 0.05 M solution precursor by sol–gel processing***", Applied physics letters, Volume 75, Number21, 1999, pp 3402-3404

21) J. J. Bock, D. Chen, P. D. Mauskopf and A. E. Lange, "***A novel bolometer for infrared and millimeter-wave astrophysics***" Space Science Reviews, Volume 74, Numbers 1-2, pp 229-235, 1995.

22) L. N. Hadley and D. M. Dennison, "***Reflection and Transmission Interference Filters***," Journal of the Optical Society of America, Volume 37, Issue 6, pp 451-453, 1947

23) L. N. Hadley and D. M. Dennison, "***Reflection and Transmission Interference Filters***," J. Opt. Soc. Am. Volume 38, Issue: 6, pp: 483-492, 1948

24) Sonalee Chopra, A. K. Tripathi, T. C. Goel and R. G. Mendiratta, ***"Characterization of sol-gel synthesized lead calcium titanate (PCT) thin films for pyro-sensors***", Materials Science and Engineering Volume 100, Issue 2, 15 July 2003, Pages 180-185

25) S.B.Lang, "***Sourcebook of pyroelectricity***", Gordon and Breach Science Publishers, 1st edition (January 1, 1974) ISBN 978-0677015804

26) S.G.Porter "***A brief guide to pyroelectric detectors***", Ferroelectrics, Volume 33, Issue 1 June 1981, pp: 193-206 Doi: 10.1080/00150198108008086

27) P. Muralt, "***Electroceramic-Based MEMS***", Electronic Materials: Science and Technology, 2005, Volume 9, Part A, pp: 81-113, DOI: 10.1007/0-387-23319-9_5

28) Muralt Paul, "***Micromachined Infrared detectors based on pyroelectric thin films***", Reports on Progress in Physics, Volume 64, Number 10, pp: 1339-1388, September 2001

29) R W Whatmore, "***Pyroelectric Devices and materials***", Reports on Progress in Physics Volume 49, Number 12, 1986

30) W. R. Blevin and Jon Geist, "***Influence of Black Coatings on Pyroelectric Detectors***," Applied Optics Volume13, Issue 5, pp 1171-1178, 1974

31) F. Jutzi, D.H.B. Wicaksono, G. Pandraud, N. de Rooij and P.J. French, ***"Far-infrared sensor with LPCVD-deposited low-stress Si-rich nitride absorber membrane—Part 1 Optical absorptivity***", Sensors and Actuators Volume 152, Issue 2, 2009, pp 119-125

32) J. J. Monzón and L. L. Sánchez-Soto, "***Optical performance of absorber structures for thermal detectors***," Applied Optics Volume 33 Issue 22, pp 5137-5141, 1994

33) Thompson, M. P., Troxell, J. R., Murray, M. E., Thrush, C. M., Mantese, J. V., "***Infrared absorber for pyroelectric detectors***", Journal of Vacuum Science & Technology A: Vacuum, Surfaces, and Films Volume: 25 Issue: 3 pp: 437 – 440, 2007

34) Silberg, Paul A. "***Infrared absorption of three-layer films***", Journal of the Optical Society of America, volume 47, issue 7, pp 575 -578, 1957

35) Parsons, A. D.; Pedder, D. J. "***Thin-film infrared absorber structures for advanced thermal detectors***" Journal of Vacuum Science and Technology A, volume 6, 1988, pp 1686-1689.

36) P. D. Mauskopf, J. J. Bock, H. Del Castillo, W. L. Holzapfel, and A. E. Lange, "***Composite infrared bolometers with Si_3N_4 micromesh absorbers***," Applied Optics volume 36 Issue 4, pp 765-771, 1997.

37) Ulrich, R. "***Far-infrared properties of metallic mesh and its complementary structure***", Infrared Physics, volume 7, Issue 1, pp. 37-50, 1967.

38) Kiewiet, F.B., Bruijn, M.P., Hoevers, H.F.C., Bento, A.C., Mels, W.A., de Korte, P.A.J., "***Fabrication and characterization of infrared and sub-mm spiderweb bolometers with low-T_c superconducting transition edge thermometers***", IEEE Transactions on Applied Superconductivity, Volume 9, Issue2 pp: 3862 – 3865, 1999

39) J. M. Gildemeister, Adrian T. Lee, and P. L. Richards, "***A fully lithographed voltage-biased superconducting spiderweb bolometer***", Applied Physics Letters, Volume 74, number 6, pp 868-870, 1999.

40) French P.J.[1]; Sarro P.M.; Mallee R.; Fakkeldij E.J.M.; Wolffenbuttel R.F., "***Optimization of a low-stress silicon nitride process for surface-micromachining applications***", Sensors and Actuators A, Volume 58, Number 2, 1997 , pp. 149-157

41) A. Tsuzuki, H. Murakami, K. Kani, K. Watari and Y. Torii, "***Preparation and ferroelectric properties of sol-gel-derived (Pb, Ca) TiO3 thin films***", Journal of Materials Science Letters Volume 10, Number 3, pp: 125-128, 1991

42) Sonalee Chopra, Seema Sharma, T. C. Goel, and R. G. Mendiratta, "***Sol–gel preparation and characterization of calcium modified lead titanate (PCT) thin films***" Ceramics International, Volume 30, Issue 7, 2004, pp 1477-1481

43) Yamaka, Eiso; Kanaya, Hiroyuki; Watanabe, Hirohito; Kimura, Hideki; Ohkuma, Haruo, "***Structural, ferroelectric, and pyroelectric properties of highly c-axis oriented Pb (1-x)Ca(x)TiO3 thin film grown by radio-frequency magnetron sputtering***", Journal of Vacuum Science and Technology A, volume 6, 1988, pp 2921-2928

BIOGRAPHICAL INFORMATION

Annand Balasubramaniyam was born in Chennai, India. He received his B.E. (2007) in Electronics and Instrumentation Engineering, from Anna University, Chennai, India. He completed his M.S degree in Electrical Engineering from the University of Texas at Arlington, in December 2010.

His research focused on design, characterization and fabrication of MEMS infrared sensor. He is interested in MEMS, Control systems, and Matlab Simulink designs.